A new assessment of the circulation of Atlantic and Intermediate Waters in the Eastern Mediterranean

Claude Estournel, Patrick Marsaleix, Caroline Ulses

Progress in Oceanography 198 (2021) 102673

Contents lists available at ScienceDirect

Progress in Oceanography

journal homepage: www.elsevier.com/locate/pocean

A new assessment of the circulation of Atlantic and Intermediate Waters in the Eastern Mediterranean

Claude Estournel *, Patrick Marsaleix, Caroline Ulses

LEGOS, Université de Toulouse, CNES, CNRS, IRD, UPS (Toulouse), France

ARTICLE INFO

Keywords:
Ocean circulation
Surface water mass
Intermediate water mass
Mesoscale features
Levantine Intermediate Water
Eastern Mediterranean Sea

ABSTRACT

A simulation of the Mediterranean circulation between 2011 and 2020 at a resolution of 3–4 km in the Eastern basin was compared to vertical profiles and horizontal distributions of temperature and salinity from Argo profilers distributed throughout the basin. The comparison is marked by high temporal (~0.9) and spatial (0.6–0.8) correlations and low biases. Comparisons of SST with satellite imagery have also shown strong similarities for numerous structures over a wide range of spatial scales. The simulation is used to describe the mean circulation of surface Atlantic Waters and Intermediate Waters in winter and summer.

The surface circulation is cyclonic alongslope, stronger and more stable in winter. In summer, the current veins are sometimes interrupted and replaced by trains of eddies like in the South Ionian. In other cases, the current becomes very narrow and stuck to the coast as along the Ionian east coast or the Middle East coast. In winter, surface and Levantine Intermediate Waters exit from the Levantine mainly through the Aegean, while in summer, they exit westward south of Crete. The Aegean tends in summer to be isolated by eddies that develop on both sides of the Cretan Arc. The juxtaposition of Ierapetra, the Rhodes Gyre and the Mersa-Matruh Eddies produces a southward path across the Levantine basin at about 27 − 28°E which delimits a large cyclonic circulation to the east which tends to separate the two parts of the basin (west and east Levantine). Concerning the Levantine Intermediate Waters, the alongslope cyclonic circulation all around the Levantine basin in winter is no longer maintained in summer as a large anticyclonic circulation occupies the southeast of the basin. The intermediate waters entering the Ionian either through southern Crete in summer or through the Aegean in winter, are submitted to a strong northward, southward and even westward dispersion by Pelops and the nearby anticyclonic areas. The presence of recurrent anticyclones between 35 and 37°N along a band extending from west to east of the Ionian also produces a vertical dispersion of intermediate water. Finally, the circulation of intermediate water in the South Ionian is marked by an important seasonality with the presence in summer of a large anticyclonic circulation that seems to be wind induced and finally drives a secondary branch to the Sicily Channel. A climatology for the transport through the different straits is discussed and simplified representations of the circulation are proposed.

1. Introduction

The Mediterranean transforms the light Atlantic Water entering the Strait of Gibraltar into denser (saltier) intermediate and deep water (Millot and Taupier-Letage, 2005) that ultimately exits the basin at Gibraltar to form a vein of water that propagates into the North Atlantic at about 1,000 m. The Mediterranean is made up of the western and eastern basins separated by the Strait of Sicily whose sill is at about 450 m. Each basin is composed of several sub-basins separated by straits or bathymetric sills. The north of the two basins is under the influence of continental winds that produce cooling / evaporation and form deep and/or intermediate waters in cyclonic gyres: the WMDW (Western Mediterranean Deep Water) in the Gulf of Lion for the western basin (MEDOC group, 1970; Testor et al., 2017), the AdDW (Adriatic Dense Water) in the South Adriatic Pit (Manca et al., 2002, Civitarese et al., 2010), the CIW (Cretan Intermediate Water) and CDW (Cretan Deep Water) in the South Aegean Sea (Georgopoulous et al., 1989, Schlitzer et al., 1991) and LIW (Levantine Intermediate Water) in the Levantine Basin for the eastern basin (Wüst, 1961); see also Hayes et al. (2019) for the main features of the circulation and properties of water masses. The

* Corresponding author at: LEGOS, OMP, 14 avenue E. Belin, F31400 Toulouse, France.
E-mail address: claude.estournel@legos.obs-mip.fr (C. Estournel).

https://doi.org/10.1016/j.pocean.2021.102673
Received 18 March 2021; Received in revised form 3 July 2021; Accepted 26 August 2021
Available online 1 September 2021

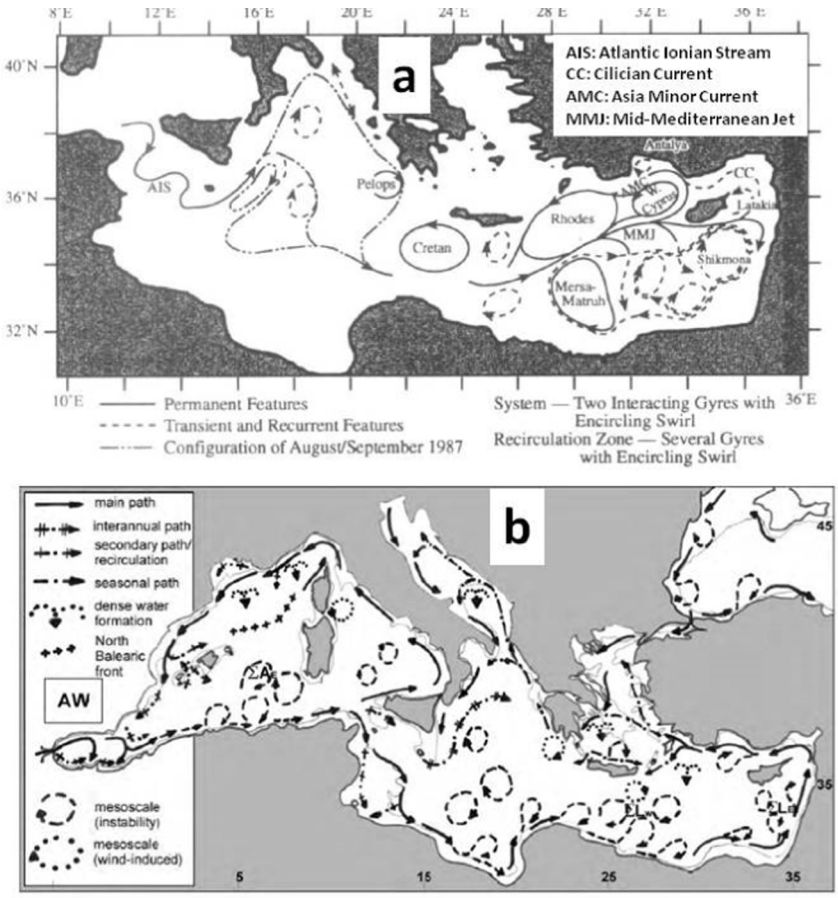

Fig. 1. Schematic of the surface circulation after (a) Robinson and Golnaraghi (1993), (b) Millot and Taupier-Letage (2005).

most striking water mass of the whole basin, a major component of the outflow at Gibraltar, is the intermediate water composed of LIW and CIW. This paper deals with the circulation of surface and intermediate waters (LIW/CIW) in the eastern basin.

1.1. *The mean circulation of the surface water of Atlantic origin*

After the remarkable pioneering study of Nielsen (1912) (see surface circulation in the Eastern Mediterranean reproduced in Hamad et al., 2006) which consists of a large alongslope cyclonic loop around the whole eastern basin, various authors in the 1960s and 1970s proposed circulation patterns and regions of water mass formation (Lacombe and Tchernia, 1960, 1972; Wüst, 1961; Ovchinnikov, 1966). Ovchinnikov (1966), whose surface circulation is reproduced in Bethoux (1980), encompassed in a cyclonic basin circulation independent cyclonic gyres in the northern Ionian, Levantine and north of the Cyrenaican coast. In the 1980s, syntheses of these works were published (Millot, 1987 for the Western Mediterranean, which was at that time the most documented basin), while the review of Malanotte-Rizzoli and Hecht (1988) for the Eastern Mediterranean, which described sporadic and sometimes even poorly documented past observations, announced the POEM campaigns whose objective was to overcome the small number of experimental and theoretical investigations in this basin. At the same time, the use of satellite images of surface temperature and ocean color allowed a more systematic view of certain characteristics of surface circulation (e.g. Arnone and La Violette, 1986).

The data of the POEM programme, which brought together numerous scientists from different countries, were obtained from 5 surveys of the eastern Mediterranean carried out on a regular network of stations between 1985 and 1987, to which were added moorings in 5 straits of the Cretan Arc as well as in the straits of Otranto and Sicily (Malanotte-Rizzoli and Robinson, 1988). The surveys targeted the Adriatic, the northern Ionian, the Levantine basin and the southern Aegean Sea. The South Ionian as well as a band about 150 km wide along the southern coast of the Levantine basin and to a lesser extent its eastern coast were thus not monitored. Different papers have examined in detail these hydrological and transient tracer observations to derive information on basin scale circulation, sub-basin scale circulation in the Ionian (Malanotte-Rizzoli et al., 1997) and Levantine (Robinson et al., 1991; Ozsoy et al., 1991), LIW formation (Ozsoy et al., 1989) and mesoscale. Circulation patterns have been produced that renew the historical patterns cited above and are still used in a wide range of publications. Based on an objective analysis of POEM observations (Robinson et al., 1991), enriched by Robinson and Golnaraghi (1993), these authors describe the general circulation of the eastern basin as "sub-basin scale gyres interconnected by jets". In this scheme (Fig. 1**a**), the characteristics named permanent are, for the gyres, the cyclonic Rhodes Gyre, West Cyprus Gyre, and Cretan Gyre and the jets are the Atlantic-Ionian Stream (AIS), the Mid-Mediterranean Jet (MMJ) and the Asia Minor Current. Thus in the Ionian, Atlantic Water leaving the Sicily Channel forms a northward anticyclonic loop (see also Malanotte-Rizzoli et al. (1997) who named it Mid-Ionian Jet - MIJ) and then continues towards the Levantine without interaction with the south of the basin to form the MMJ which flows from southwest to northeast in the center of the basin and joins the Asia Minor Current. The southeast of the Levantine, from 27°E and much of the Middle East coast (up to the south of Cyprus) left out by the basin-scale circulation, is occupied by so-called recurrent or transient high pressure areas resulting in a large isolated anticyclonic region, the eastern branch of which is an along slope current directed from northeast to southwest.

Later, Millot and Taupier-Letage (2005) described the circulation of surface (Fig. 1**b**), intermediate and deep water in the western and

eastern basins based on sea surface temperature (SST) images and in-situ observations, and derived similarities and differences between these two basins summarized here. Overall, each basin has an alongslope cyclonic circulation that describes a basin-wide gyre, although the western basin is a transition basin for Atlantic Water, much of which escaping into the eastern basin. The two gyres are constituted in the south by an alongslope current which is more or less unstable along the different portions of the coast, (the most unstable ones are the Algerian Current in the west and the Libyo-Egyptian Current in the east), thus developing anticyclonic eddies which disperse northward part of the Atlantic Water. This description was developed in various papers that are largely based on the analysis of a large number of SST images (Hamad et al., 2005, 2006).

The northern shores of the two western and eastern basins differ due to the much more complex configuration of the eastern basin, which does not allow the development of the equivalent of the Northern Current, component of the general circulation following the entire northern coast of the western basin (Sammari et al., 1995). On the other hand, in both basins, the alongslope current is more stable than in the south. The extreme case is the Northern Current, which develops meanders but rarely detaches eddies, whereas along the Turkish coast bordering the northern part of the Levantine basin, eddies of a few tens km in diameter are formed along the Asia Minor Current according to Millot and Taupier-Letage (2005). These latter authors explained that the surface water from the Asia Minor Current divides into 2 veins (Fig. 1b), one of which enters the Aegean Sea through the straits of the Cretan Arc and thus participates in the basin scale gyre of the entire eastern basin, the other remains in the Levantine basin flowing along the Arc up to Crete forming the northern branch of the Rhodes Gyre, then without progressing further west, recirculates cyclonically to ultimately end as the first branch into the Aegean. In the Aegean Sea, the Levantine Surface Water (corresponding to the surface Atlantic Water that have turned warm and salty due to strongly positive heat balance and strong evaporation in summer/fall) follows two cyclonic paths that both end in the Ionian, passing through the western straits of the Cretan Arc, the first one skirts the South Aegean and the second one flows in the North Aegean along the Turkish coast and then joins the Black Sea Water flowing southward along the west coast of the Aegean. The surface Water at the exit of the Ionian then heads north to complete its cyclonic course, one part bypassing and the other entering the Adriatic along the eastern flank of the Otranto Strait and making a cyclonic circuit around the basin or around the South Adriatic Pit. Millot and Taupier-Letage (2005) pointed out that the surface water vein after closing its circuit around the eastern basin joins in the southeast of Sicily the younger vein which leaves the Sicily Channel to start again the whole cyclonic circuit.

Finally, more recently, Menna et al. (2012) and Menna et al. (2020) proposed a scheme of the surface circulation in the Levantine based on geostrophic currents deduced from drifter and altimetry, which indicates the coexistence of an alongslope cyclonic circulation as in Millot and Taupier-Letage (2005), and of the Mid Mediterranean Jet of Robinson and Golnaraghi (1993).

1.2. The circulation of intermediate water (LIW/CIW)

According to Millot and Taupier-Letage (2005), intermediate water (LIW + CIW see above) characterized by a salinity maximum in the subsurface, also flows cyclonically in the eastern basin but exits at the Sicily Strait, after which it follows a cyclonic course in the Tyrrhenian Sea and then around the Algero-Provençal basin to the Alboran Sea and the Strait of Gibraltar. Debates exist on the areas of formation of LIW. A general consensus gives the Rhodes gyre as the main area of formation (Lascaratos and Nittis, 1998) but different authors also argue for the Turkish coast (Kubin et al., 2019; Fach et al., 2021), the Israeli coast, or even the whole basin (see Lascaratos et al., 1993; Ozsoy et al., 1993). This question deserves a great deal of attention but is beyond the scope of this paper. According to Millot and Taupier-Letage (2005), the differences with the surface Water course lie north of the Levantine basin and the Aegean. In the first case, the section of the straits of the eastern Cretan Arc at intermediate depths would only allow part of the LIW to flow through, with most of it continuing along the south coast of Crete towards the Ionian. For the same reasons, in the Aegean, LIW would preferentially flow around the South Aegean to exit with the CIW through the western straits.

Malanotte-Rizzoli et al. (1999) based on the analysis of data from the 1987 (POEM-AS87) and 1991 (POEMBC-O91) POEM campaigns showed a high variability in the path of intermediate waters. In 1987, the LIW after flowing along the coast south of Crete divided into two branches, one circulating around the Ionian as in Millot and Taupier-Letage (2005) and the other bypassing this course to head towards the Sicily Channel. In 1991, on the other hand, the path was much more complex. The LIW remained blocked in the Levantine basin due to the presence of intense anticyclonic eddies and it is the CIW that would circulate towards Sicily by the South due to a blockage of the path towards the North Ionian.

1.3. Internal variability and climatic variability

This is certainly the moment to introduce a breakpoint with the Adriatic-Ionian Bimodal Oscillating System - BiOS, which consists of a decadal (cyclonic/anticyclonic) reversal of the surface and intermediate Ionian circulation, shown from time series of salinities and sea level anomalies (Gacic et al., 2010). Numerous papers have followed to illustrate (Velaoras et al., 2014; Bensi et al., 2016; Kokkini et al., 2020) or interpret (Gacic et al., 2011; Theocharis et al., 2014; Krokos et al., 2014) this major feature. New circulation patterns have thus emerged for both Atlantic and Intermediate Waters. In anticyclonic conditions, Atlantic Water at the outlet of the Sicily Channel enters the North Ionian, producing saltier surface waters in the Levantine Basin, which favors the formation of salty LIW (see maximum salinity of LIW in the southeast of the Levantine Basin in Ozer et al. (2017) corresponding to the peaks of the anticyclonic phases of the BIOS). Surface and intermediate waters at the exit of Aegean are then pushed back by the Ionian anticyclonic circulation and head directly towards the Sicily Channel. This situation corresponds for the Ionian to the description of Malanotte-Rizzoli et al. (1999) for the 1991 POEM campaign (see Fig. 10b of the latter paper), which, by extrapolating the time series of Gačić et al. (2014) which unfortunately begins in 1993, would indeed indicate an anticyclonic period. The situation described by Millot and Taupier-Letage (2005) of an eastward path of Atlantic Water in the southern Ionian bypassing the northern Ionian, would correspond to the BIOS cyclonic phase during which the Atlantic Water strongly impacts the surface salinity of the Levantine basin, probably reducing the formation of intermediate waters which, at the exit of the Aegean, are transported by the Ionian cyclonic circulation all around this basin and towards the Adriatic. It thus seems that the BIOS allows, at least for the Ionian, to reconcile the two circulation patterns as representative of its two anticyclonic and cyclonic phases. It should be noted that the representation of the BIOS by models remains a challenge as summarized by Menna et al. (2019a).

We only briefly mention the Eastern Mediterranean Transient (EMT), a major event of the early 1990s that resulted in a massive flow of very dense water produced in the Aegean Sea to the rest of the deep basin. The consequences of this event have mainly affected deep waters which are beyond the scope of this paper.

1.4. Mesoscale circulation

The presence of numerous mesoscale structures in the eastern basin is a consensus. Satellites and in particular altimetric sensors have been massively used to characterize them. Mkhinini et al. (2014) from a detection of eddies in gridded AVISO altimetry products over 20 years showed that 80% of eddies with a lifetime greater than one year are anticyclonic, and anticyclones are larger on average than cyclones. Sorgente et al. (2011) and Jebri et al. (2016) listed the recurrent structures of the Sicily Channel with cyclones along the south coast of

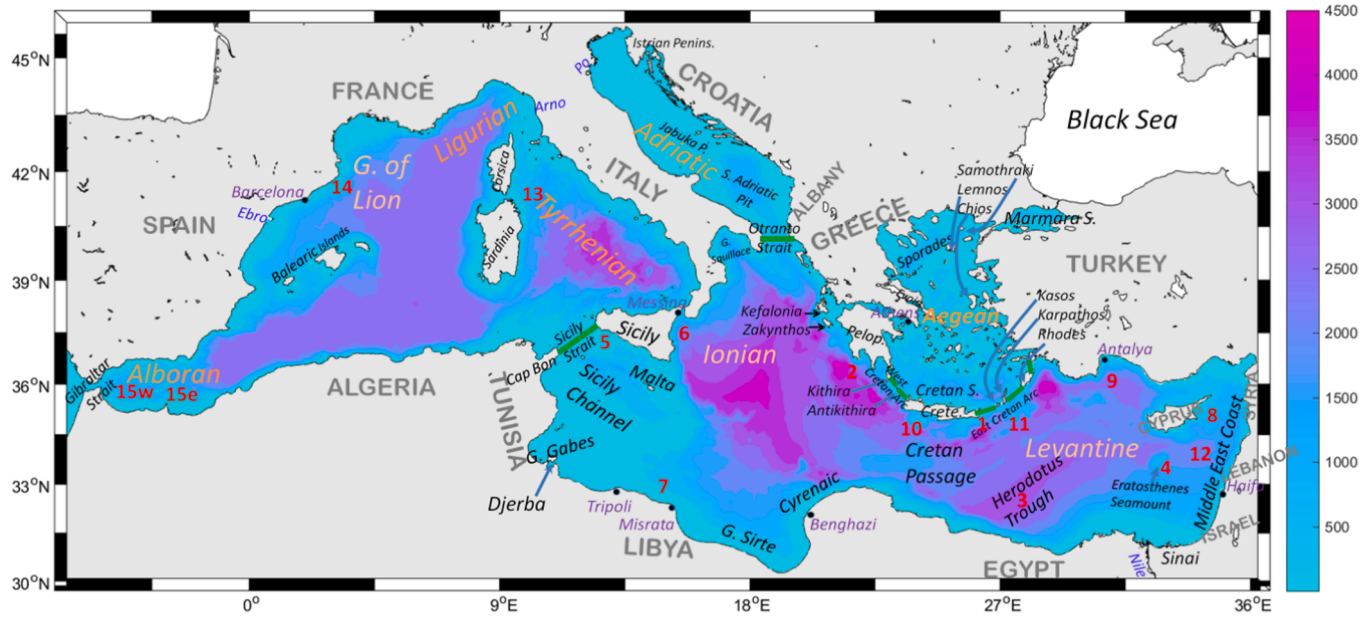

Fig. 2. Bathymetry of the Mediterranean used in the simulation. The names of the places mentioned in the text are shown in the figure. The numbers in red correspond to the locations of eddies or gyres named in the text: 1: Ierapetra ; 2: Pelops ; 3: Mersa-Matruh Eddies ; 4: Cyprus Eddy ; 5: Adventure Bank Vortex ; 6: Messina Rise Vortex ; 7: Sidra Gyre ; 8: Latakia Eddy ; 9: Antalya Eddy; 10: Cretan Cyclone; 11: Rhodes Gyre; 12: Shikmona; 13: Bonifacio Gyre; 14: Pyrenees Front; 15w and 15e: Western and Eastern Alboran Gyres. The green lines indicate the straits through which the transport has been calculated (section 4.4).

Sicily possibly related to bathymetry (Fig. 2) such as the Adventure Bank Vortex or to the northeast the Messina Rise Vortex which would also be induced by the wind (Menna et al., 2019b). Anticyclonic structures are also noted in the South Ionian such as the Sidra Gyre or a large summer anticyclonic structure stretched from 14° to 17°E (Gerin et al., 2009) and which, according to Menna et al. (2019b) would in fact correspond to the Sidra Gyre involving two smaller anticyclonic structures.

Moving from the Ionian to the Levantine basin, the two anticyclones of Pelops and Ierapetra to the northwest and southeast of Crete with a diameter of about 100 km are known to be forced by the curl of the northerlies Etesians blowing from the Aegean and accelerated around relief (Peloponnese for Pelops, and between Crete and Kasos for Ierapetra). Ierapetra can last several years (sometimes reactivated each summer) and it can also move and merge with other anticyclones (Ioannou et al., 2017). Besides these eddies that are deterministic in their place of appearance and long-lasting (they are sometimes described as permanent), many anticyclones do not seem to be related to the wind but rather to the instability of the slope current. A first zone of formation of small and short-lived anticyclones was named by Mkhinini et al. (2014) Benghazi Eddies around 20°E. Further east, Mkhinini et al. (2014) and Gerin et al. (2009) noted the recurrent presence of anticyclones in the Herodotus Trough which they finally named Herodotus Trough Eddies which include the anticyclone classically named Mersa Matruh (Hamad et al., 2005) or sometimes Egyptian Eddy (Menna and Poulain, 2010). This “structure” corresponding either to an accumulation of locally or upstream formed eddies and sometimes even Ierapetra, was named by Millot and Taupier-Letage (2005) “SLw” (accumulation in the western Levantine) and attributed to the shape of the deep isobaths that would trap the eddies in this pit. In the following, we retain the frequently used name Mersa-Matruh. Similarly, the latter authors note “SLe” an accumulation of anticyclones in the southeastern Levantine including the classic Shikmona or Cyprus Eddy formed over the Eratosthenes seamount in southern Cyprus (Zodiatis et al., 2005). Along the northeast coast of the Levantine Basin, the Asia Minor Current produces eddies with a shorter life span (Fach et al., 2021) such as the anticyclonic Antalya Eddy.

1.5. Contribution of numerical modeling

Most of the results detailed above are derived from in-situ and satellite observations. Of course, numerical modeling has been widely used for at least forty years and with a strong increase in efficiency due to the growth of computing power. Modeling can be broken down into different axes, according to spatial scales, basin models, sub-basin models, coastal models, and temporal scales, process oriented models, seasonal, interannual or climatic studies. Finally, the use of different data assimilation techniques makes it possible to have short-term analyses or reanalyses, a compromise between fully satisfying the equilibria of geophysical fluid mechanics and reducing the discrepancies with the observations predominant at the surface thanks to the coverage of satellites, although Argo profiles are a factor of improvement also at depth.

Models that deal with the entire Mediterranean basin and thus provide an overall consistency of horizontal and vertical circulation and exchanges of water, heat and salt, usually have a horizontal resolution of 1/8° (Beuvier et al., 2010; Somot et al., 2016), 1/12° (Beuvier et al., 2012; Macias et al., 2019) and 1/16° (Béranger et al., 2005; Sannino et al., 2014; Pinardi et al., 2015). These resolutions for the Mediterranean are considered eddy permitting (Soto-Navarro et al., 2015), i.e. the models are limited in mesoscale reproduction although 1/16° allows the representation of large eddies in the Levantine basin (Alhammoud et al., 2005). Moreover, with a few exceptions (Beuvier et al., 2010; Béranger et al., 2005; Macias et al., 2019; Pinardi et al., 2015), the papers produced with these models do not systematically show the basin circulation, frequently focusing on different metrics developed to compare climate models such as the inflow/outflow at Gibraltar (Soto-Navarro et al., 2015) or the mean thermohaline characteristics (Soto-Navarro et al., 2020).

This panorama shows that a detailed analysis of high-resolution simulations at the scale of the Mediterranean basin could be useful to contribute to a better knowledge of the basin circulation. A prerequisite is that these simulations are carefully compared with the observations which are booming since the Argo era. We believe that the water masses circulation, despite the little attention it has received in the last 10–15 years, is an important issue, especially for environmental applications which are increasingly the scientific and societal priorities (e.g.

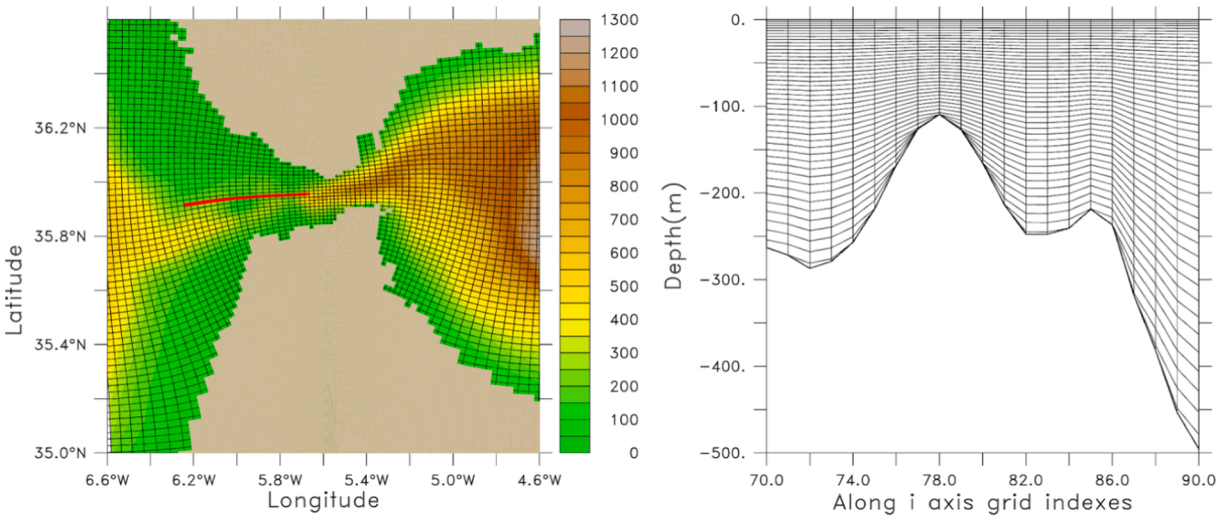

Fig. 3. Left: Bathymetry of the Strait of Gibraltar. The black lines are the axes of the horizontal curvilinear grid. Right: axes of the grid in a vertical plane whose horizontal location is given by the red line in the figure on the left.

ecosystems, resources, carbon cycle, microplastics, pollutants). This paper aims to fill this gap by presenting over the Eastern Mediterranean a simulation of about a decade at a resolution of 3 to 4 km assessed from about 25,000 Argo profiles. We focus on the 10-year averaged seasonal surface and intermediate circulation including a significant contribution from recurrent mesoscale structures. The simulated circulation is described and compared with the bibliography. Transport diagnostics in the different straits between sub-basins are then presented. Finally, simplified schemes of seasonal circulation of surface and intermediate waters are provided.

2. Methods

2.1. The SYMPHONIE model and its forcings

We use the 3D primitive equations SYMPHONIE described in Marsaleix et al. (2008, 2006), Damien et al. (2017), with turbulence closure and convection parameterization detailed in Estournel et al. (2016). More details, on the one hand on the validation of the model in the Mediterranean, and on the other hand on applications to biogeochemistry in relation to the formation of dense water masses, can be found in Estournel et al. (2003, 2005); Herrmann et al. (2008); Seyfried et al. (2017, 2019); Kessouri et al. (2018); Ulses et al. (2021).

The modelled domain covers the whole Mediterranean Sea and the Marmara Sea and extends westward up to 8°W in the Gulf of Cadiz. A horizontal curvilinear grid is used which progressively increases from about 2 to 4.5 km from northwest to southeast in accordance with the increase of the Rossby deformation radius. More locally, a narrowing is carried out at the Gibraltar strait with a 1.3 km grid in order to improve the representation of this major area for exchanges with the Atlantic (Fig. 3, left). An accurate representation of the inflow/outflow depends indeed on a faithful representation of the section of the strait. The vertical grid has 60 levels. The VQS (vanishing quasi-sigma) vertical coordinate concept described in Dukhovskoy et al. (2009) is used to avoid an excess of vertical levels in shallow areas (Fig. 3, right) while maintaining an accurate description of the bathymetry and reducing the truncation errors associated with the sigma coordinate (Siddorn and Furner, 2013, Graham et al., 2018). Its implementation (see Appendix A) preserves the horizontal continuity of the fields without the blocking effect of staircase coordinates. The bathymetry is built from the GEBCO database. Fig. 2 shows the bathymetry of the Eastern Mediterranean as specified in the model. The names of geographical landmarks specified in the text are also indicated.

The model is initialized from an analysis produced by the operational oceanography center MERCATOR OCEAN International, MOI (Lellouche et al., 2013). As stratification is crucial for mesoscale characteristics, the stratification has been debiased from observations collected over the whole basin as in Estournel et al. (2016) while preserving the first hundred meters which benefits optimally from the data assimilation performed at MOI. MOI's analyses are then used to force the model to the western boundary throughout the simulation. The SYMPHONIE run is free (without any data assimilation). In the Marmara Sea, exchanges with the Black Sea are introduced at the level of the Bosphorus by a net flow of 300 km3/year according to Unluata et al. (1990) to which a seasonal cycle according to Tugrul et al. (2002) is superimposed. The initial profiles in the Marmara Sea being very different from the climatological values, we introduced a relaxation with a characteristic time of 3 days during the first 10 days, then 20 days thereafter towards a temperature of 14.5 °C and a salinity of 38.6 for depths>22 m. These values, reflecting the 2-layer structure typical of the Marmara Sea, are derived from observations near the Dardanelles Strait (Tugrul et al., 2002) for salinity and from Unluata et al. (1990) for temperature.

Air-sea forcing is an essential component of the modeling system from which the general circulation will result, in particular the cyclonic gyres (Herbaut et al., 1997; Pinardi and Navarra, 1993) or the dense water formations that maintain the intermediate and deep circulation, and in some cases, the mesoscale eddies induced by the wind curl. Alhammoud et al. (2005) indicated for example that the Ierapetra eddy is not reproduced by their model because of the too coarse resolution of atmospheric forcing. The high resolution of the air/sea forcing was thus a priority for our study, which led us to use the hourly forecasts of ECMWF since December 2011 (previously 3-hourly) at the horizontal resolution of 0.125° (an increased resolution is available since 2016 but we have chosen to keep it constant over the whole run). The turbulent heat and momentum fluxes are calculated by bulk formulas. Seyfried et al. (2017) compared with a high-resolution coupled ocean–atmosphere model, three bulk parameterizations on the case of convection in the Gulf of Lion over the winter 2012–2013. They found an uncertainty by a factor of 2 on the volume of water formed. It is obvious that on a multi-year simulation, the consequences of such uncertainties are drastic. We therefore carried out sensitivity tests based on the COARE3.0 parameterization (Fairall et al., 2003). For this, we compared the evolution of the stratification of the intermediate and deep waters simulated and observed with a particular attention to the southern Adriatic basin which showed a rapidly evolving dynamics over the last decade (Kokkini et al., 2020 for the period 2013–2016 and this study from 2017). The

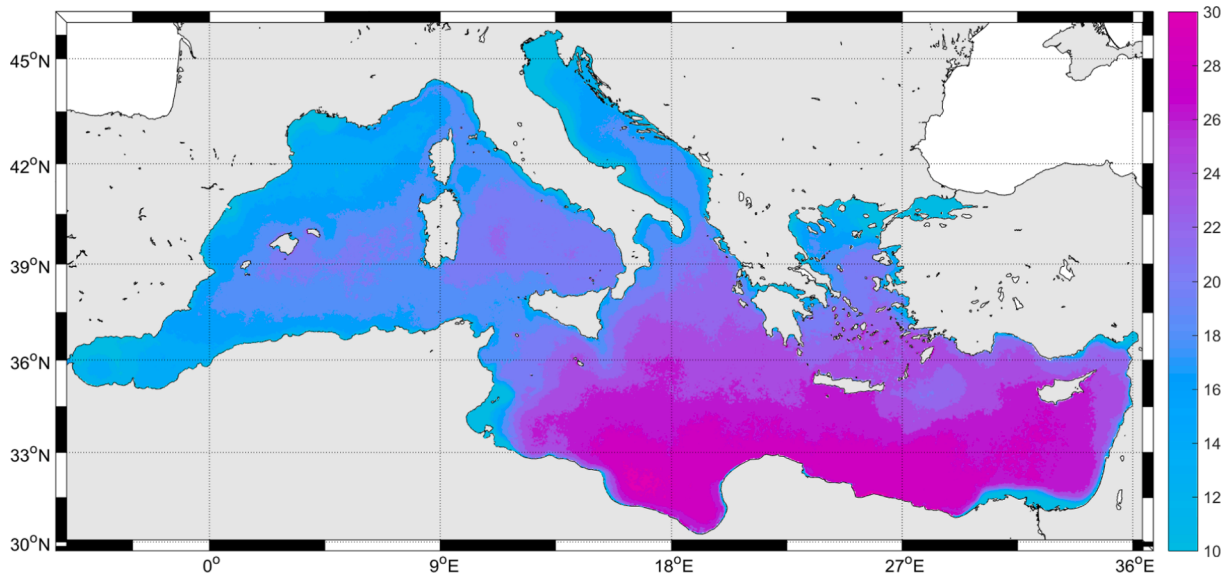

Fig. 4. Inverse of the extinction coefficient (in meter) derived from satellite product and calibrated for this study.

sensitivity tests explored the increase in these fluxes in strong wind conditions (the most uncertain cases for the parameterizations). At the end of these tests, we opted for a linear increase of the drag coefficients for momentum, heat and water following (1):

$$C_d = C_d \cdot (0.125 \cdot max(V, 11) - 0.375) \quad (1)$$

resulting in a factor of 1 (no increase) for wind speeds V lower than 11 m/s and of 1.5 at 15 m/s.

We deduced from satellite observations a parameterization of the solar flux penetration in the surface layers. Classically, the solar flux is divided into two bands, one of which is absorbed/scattered over the first tens of centimeters and the second between 400 and 700 nm over a typical thickness of 20 m (Paulson and Simpson, 1977). We used classical values for the most superficial layer that would capture 58% of the total solar flux and an attenuation depth (exponential law) of 35 cm. For the deeper extinction which concerns 42% of the solar flux, we averaged over 3 years the monthly averages of the OLCI Diffuse Attenuation Coefficient at 490 nm (product Copernicus Marine Service: OCEANCOLOUR_MED_OPTICS_L4_NRT_OBSERVATIONS_009_039) then we interpolated this field on the model grid. These data reflect the well-known behavior of the water transparency in the Mediterranean which increases from west to east and is reduced in coastal areas. After some tests and comparisons with temperature profiles in the Gulf of Lion and in the Levantine Basin, we produced an adjustment of these values according to Eq. (2) which, moreover, specifies minimum and maximum values of 10 and 30 m for the depth used in the exponential attenuation law:

$$Kd_{model}^{-1} = Max\left(Min\left(0.9 \times \left(Kd_{sat}^{-1} - 2\right), 30\right), 10\right) \quad (2)$$

Fig. 4 presents the inverse of the attenuation coefficient K_d.

The simulation is also forced by tides with 9 tidal waves (M2, M2, S2, K2, K1, O1, P1, Q1, M4). We used the tidal generating potential, as in Pairaud et al. (2008) and, at the Atlantic open boundary, the harmonic analysis of FES2014, a global finite element spectral model that assimilates altimetry and tide gauges (Lyard et al., 2021).

A total of 124 rivers are considered in the Mediterranean and 6 in the Gulf of Cadiz. As often as we have found discharge measurements, we have imposed daily values, namely for 10 French rivers as well as for the Ebro, Arno and Po rivers. For the other rivers of the Spanish and Tyrrhenian coasts, as well as Algeria and Tunisia, constant values have been introduced according to different sources including Wikipedia. For the Aegean Sea, we introduced the rivers indicated by Poulos et al. (1997) for the Greek and Turkish coasts and some secondary rivers. A climatology was applied according to the average curve corresponding to the Greek rivers given by the latter authors. The same treatment was applied to the rivers of the Levantine basin outside the Nile for which a constant value of 475 m3/s estimated by Nixon (2003) after the Aswan damming was prescribed. The most complex case is the Adriatic as it receives about 30% of the inputs to the Mediterranean (Ludwig et al., 2009) which modulate the deep and coastal dense water formation. Verri et al. (2018) showed that dense water formation in the southern Adriatic and the density of the water outflow towards the Ionian is sensitive to river inputs and Janekovic et al. (2014) indicated that models were not able to represent coastal dense water formation on the eastern Adriatic coast due to overestimation of river discharges along this coast. According to Ludwig et al. (2009), total freshwater discharge to the Adriatic would have been 127 and 118 km3/year for the 1960s and 1990s respectively, while Verri et al. (2018) gave an average estimate of 141 km3/year. For our part, we have selected the 26 most important rivers in addition to the Po. The average discharges of these rivers were increased to represent the minor rivers and bring the total average flux over 2012–2019 (north of 40°N) to 137 km3/year. These discharges have been modulated by the monthly climatology of the Po River reconstructed from the daily discharge over the period 2011–2020.

In total, mean annual riverine inputs to the Mediterranean are in our simulation 277 km3/year, 15% lower than the value of 328 km3/year given by Ludwig et al. (2009) for the decade 1991–2000.

2.2. Observations and diagnostics

The behaviour of the model at the scale of the whole Mediterranean basin is first evaluated from SST images. The L3S product from Météo-France distributed by Copernicus Marine Service (SST_EUR_SST_L3S_NRT_OBSERVATIONS_010_009_a) is used.

Argo profiles were collected on the Coriolis website (http://www.coriolis.eu.org/) over the simulation period and over the whole Mediterranean, *i.e.* 25,000 profiles over the eastern basin. Each profile is compared to the profile simulated on the same day and interpolated to its position. These profiles are referred to as "simulated Argo". The comparisons are then presented in temporal and spatial form. Three diagnostics are established:

- Mean profiles and their standard deviations are calculated at the basin and sub-basin scale,

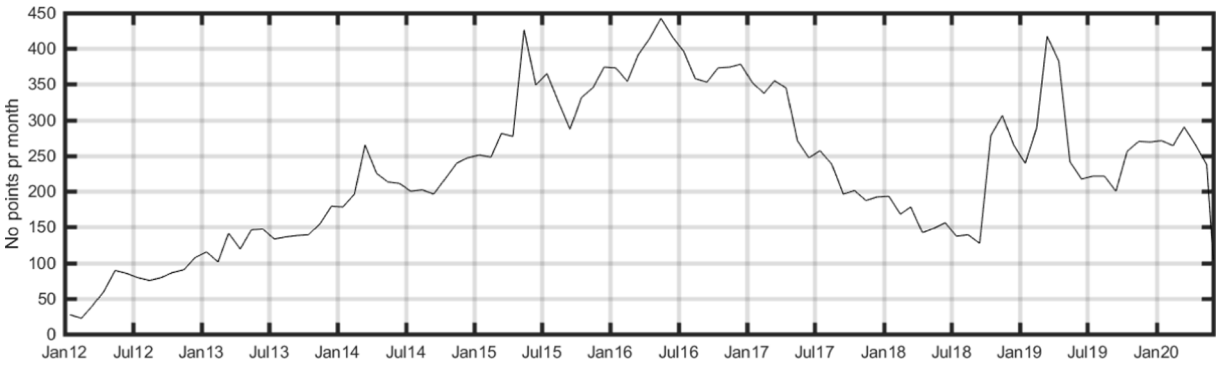

Fig. 5. Number of Argo profiles available for each month.

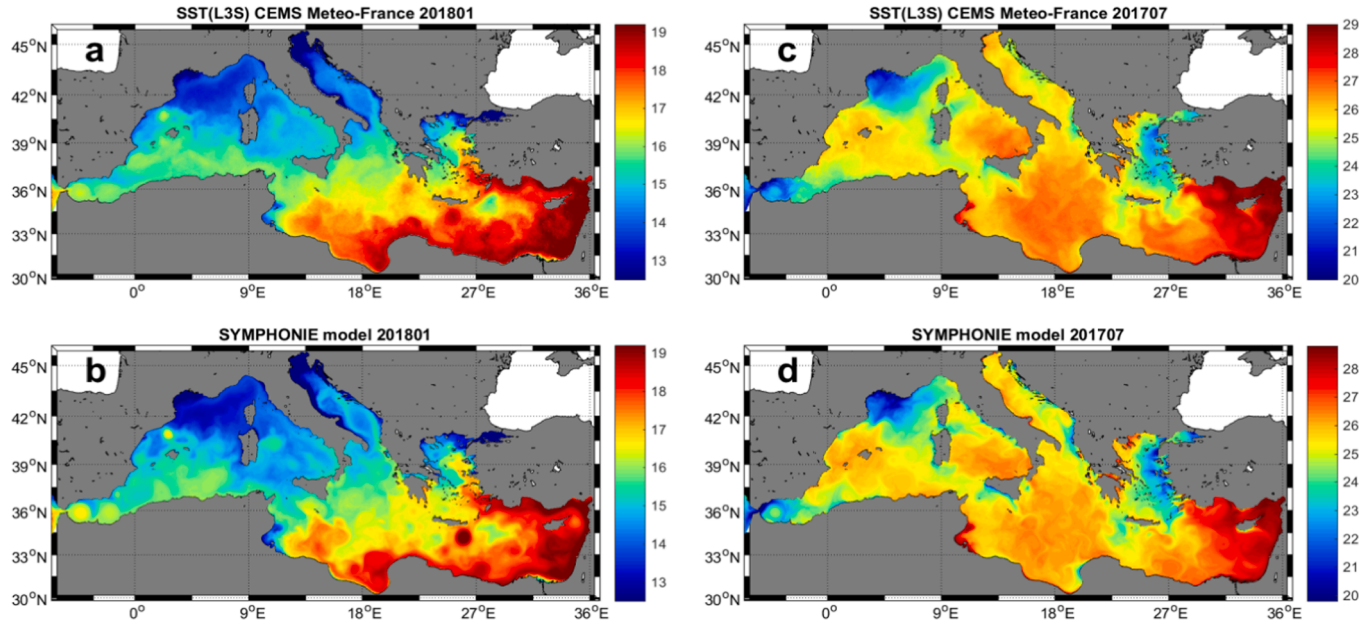

Fig. 6. Sea surface temperature averaged over one month from the satellites (a and c) and the model (b and d). Left: winter (January 2018), right: summer (July 2017). Note that the colorbar of the model has been shifted by −0.2 °C for summer to facilitate the comparison.

- In order to evaluate the temporal evolution of the simulation, we compare the time series of the observed and simulated monthly averages,
- In order to evaluate the spatial representation of the hydrology, all the observed and simulated values are mapped and compared at a few depths.

For the last two steps, correlation and bias are given. We chose to compare salinity and temperature in the surface (20 m), intermediate (225 m) and 800 m layers (excluding the temperature at 20 m strongly affected by the annual cycle which gives correlations very close to 1). For these diagnostics, the Levantine basin is defined as the region east of 25.3°E. The South Aegean is considered south of 38°N. Both are delimited by the Cretan Arc. The southern limit of the Adriatic is taken at 40°N. Finally, Fig. 5 shows the monthly distribution of the Argo profiles with an optimum in 2016 followed by a decrease fortunately partially filled in autumn 2018 by the PERLE experiment (see objectives in https://campagnes.flotteoceanographique.fr/campagnes/18000865/) .

3. Evaluation of the simulation

3.1. Evaluation with the SST

The simulation is initialized in May 2011 and ends in May 2020. Before focusing on the eastern basin, we verify the functioning of the model at the whole Mediterranean scale. The daily images are interpolated on the model grid and then averaged over one month (each pixel represents the average of cloudless pixels). The daily surface temperature of the model is averaged over the whole month. Fig. 6 shows the comparison over a winter month (January 2018) and a summer month (July 2017). The years were chosen to maximize the number of cloudless pixels in the 2016–2019 period (far from the model initialization).

In both seasons, the simulation represents the large-scale features present in the satellite images but also various smaller structures. In winter, the northern part of the Western, Adriatic and Aegean basins is cold. Cold temperature is also a tracer of cyclonic gyres in the northwestern Mediterranean, the South Adriatic Pit and Rhodes Gyre while warm temperature characterizes the two anticyclonic Western and Eastern Alboran gyres. The cold convection zone of the Gulf of Lion and the Ligurian Sea is bordered to the north by the warmer Northern Current which forms the northern part of the cyclonic gyre and similarly for the Rhodes Gyre bordered to the north along the Cretan Arc by a narrow

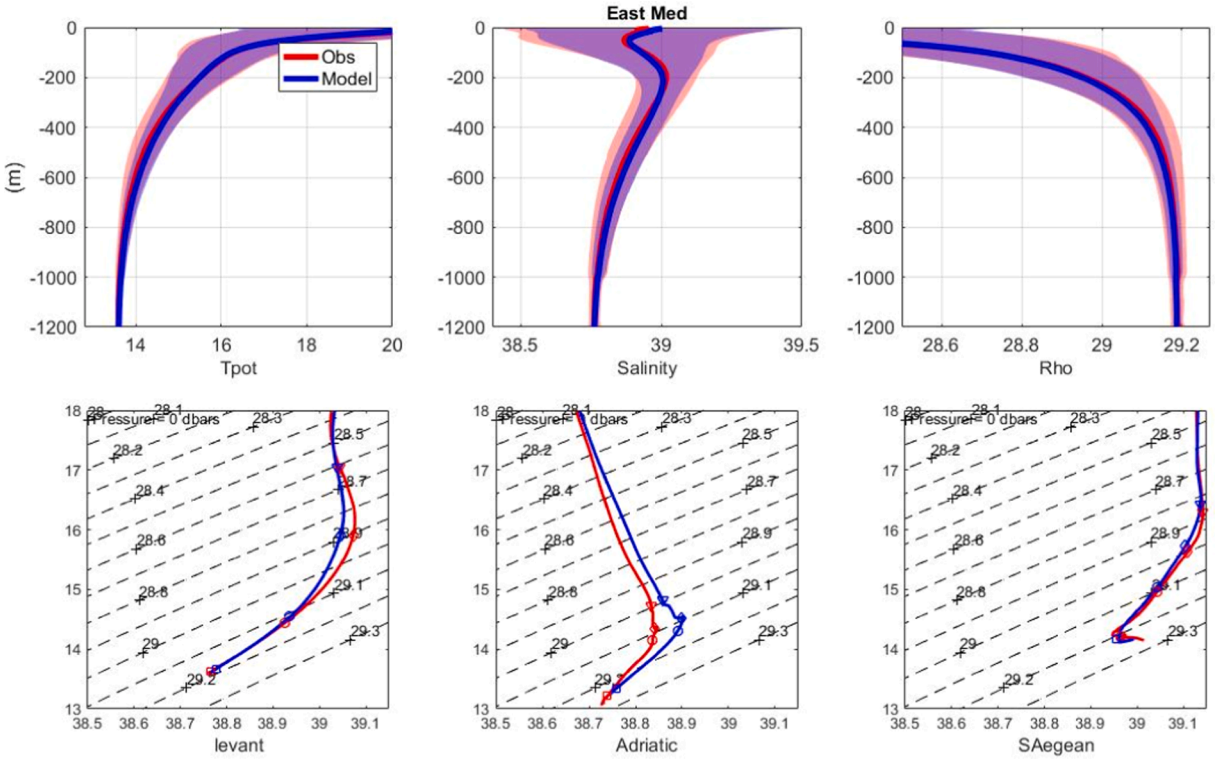

Fig. 7. (top) Mean profile and standard deviation of potential temperature, salinity and density observed (red) and simulated (blue) over the entire eastern basin. (bottom) T/S diagram observed (red) and simulated (blue) averaged over the Levantine, Adriatic and South Aegean basins and presented here between the surface and 1200 m. The simulated profiles are taken at the same positions and for the same times as the observations. The symbols on the diagrams correspond from the densest to the least dense at depths of 1000, 400, 200 and 100 m.

warm current. The model reproduces the presence of an anticyclonic eddy in the Balearic Sea near Barcelona (40.7°N 2.2°E) similar to that observed in 1998–1999 and reported as an exceptional event by Pascual et al. (2002). In the south, the temperature increases from west to east with the exception of the region of Sfax and the Gulf of Gabes to the island of Djerba because of their shallow depth as noted by Millot and Taupier-Letage (2005). A very strong thermal gradient is established between the latter region and Tripoli (Libya) where a warm band starts and further follows the entire coast up to the northeast of the Levantine Basin and the east of the South Aegean. In both satellite and model, eddy structures are visible. For example, the Libyan coast between Tripoli and Misrata is characterized by extensive anticyclonic development corresponding to the Sidra Gyre. The Egyptian coast is also characterized by eddies that indicate current instability. Under Crete and Peloponnese, the two major anticyclones of the basin are present, Ierapetra and Pelops, the last one less visible in the simulation.

In summer, the surface characteristics are very different from winter, but strong similarities are clear between the satellite and the simulation. The cold area of the northwestern Mediterranean is much less extended than in winter, its shape is very well reproduced by the simulation. To the southwest of the Gulf of Lion, a very marked front, called the Pyrenees Front (García et al., 1994), separates the cold water of the Gulf of Lion from the warm water of the Balearic Sea. The anticyclonic gyres of the Alboran Sea associated with an upwelling on the Spanish coast to the north whose cold water is advected to the Algerian coast are clearly visible. In the north of the Tyrrhenian, the cold waters of the cyclonic gyre of Bonifacio between Corsica and Sardinia are observed and simulated. In the eastern basin, the cold areas correspond to upwelling, along the eastern coast of the Aegean, along the Albanian coast, stuck to the coast south of Benghazi, south of Cyprus and south of Sicily with the Maltese filament that develops in the southeast corner and is advected southeastward towards the Libyan coast. These upwelling are generally well reproduced by the simulation both qualitatively and quantitatively. There are also much smaller scale structures also generated by the wind, for example downwind blowing through the Strait of Messina or the anticyclone further northeast in the Gulf of Squillace. It is also interesting to see two cold areas, on either side of Crete, that stretch southward and are linked to the Etesians (and to the west to a convergence with a northwest wind blowing along the Ionian coast). To these winds are associated two symmetrical eddy structures, one cyclonic at the southwest corner of Crete and Ierapetra anticyclonic at the southeast corner, the latter not discernible on the SST but present on the sea surface height of the model as well as the Rhodes gyre. Many other eddies populate the Levantine Basin along Egypt, south of the Gulf of Antalya or along the Middle East coast but they are more difficult to discern in summer. Finally, we can see that in the south-eastern Aegean Sea, unlike in winter, the penetration of Levantine surface water seems to be completely prevented at the surface by upwelling and/or wind both in the satellite and simulation.

3.2. *Evaluation with the Argo profiles*

The comparison with the Argo observations starts on January 1, 2012. Fig. 7 presents the mean potential temperature, salinity and potential density profiles and their standard deviation over the whole eastern basin as well as the mean T/S diagrams observed and simulated over the three main water mass formation zones, the Adriatic where AdDW is formed, the South Aegean where CIW and CDW are formed and the Levantine where LIW is formed.

At the scale of the eastern basin, the Atlantic Waters are characterized by a minimum of salinity in subsurface at a depth of 50 m. The latter is present in particular in summer and autumn and mainly in the south of the basin. Indeed, in the Levantine basin (representing about 40% of the Argo profiles), a distinction is made between the warm and salty Levantine Surface Water (not shown on the T/S diagram), and the less salty Atlantic Water present around 50 m deep (see more details in Fig. 9

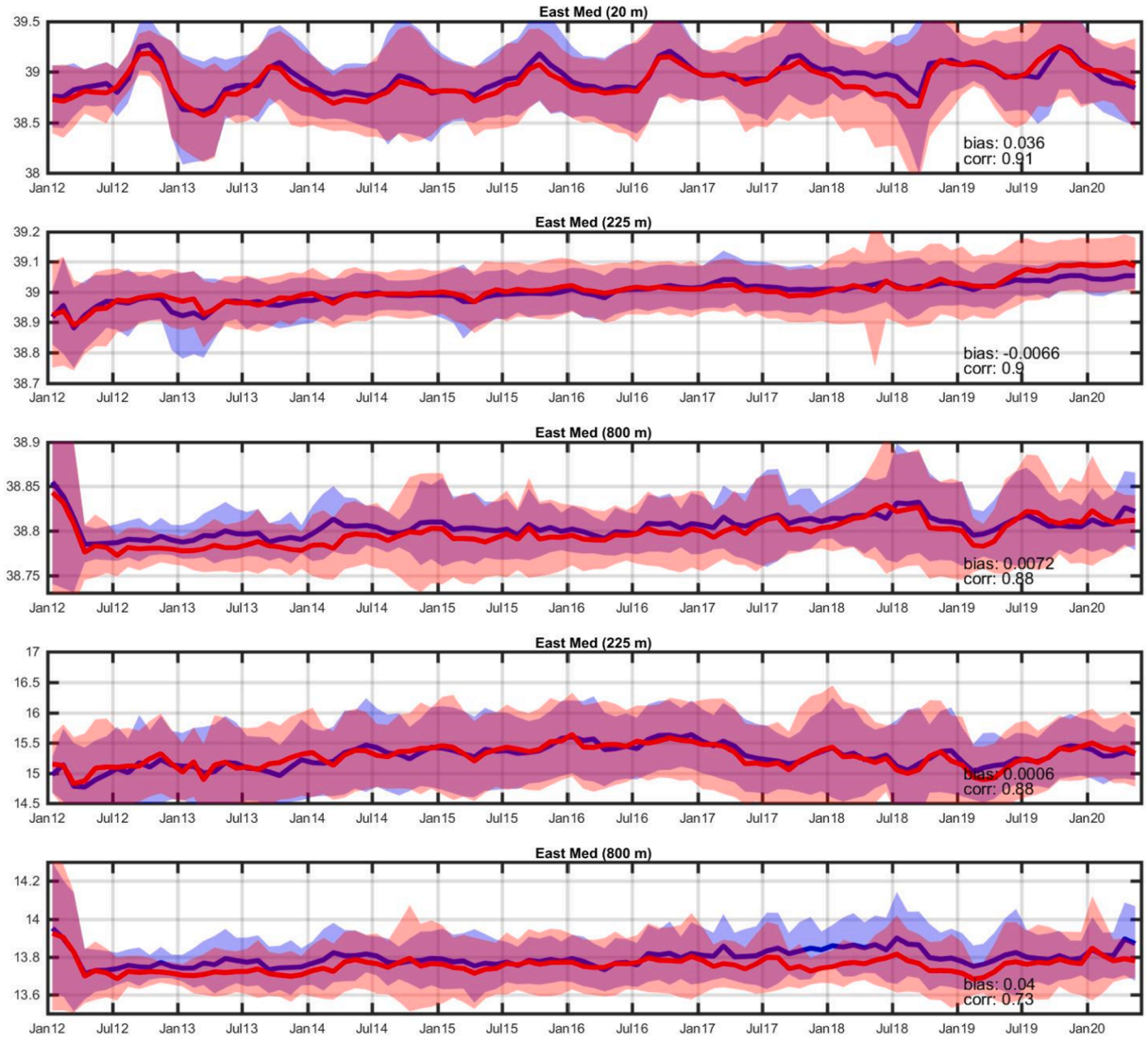

Fig. 8. from top to bottom, temporal evolution of monthly mean salinities at 20, 225, 800 m and temperatures at 225 and 800 m extracted from observed (red) and simulated (blue) Argo profiles. The bias and correlation of the two curves are shown in the figures.

which presents a seasonal analysis). At 200 m, the average profile is marked by the maximum salinity of the intermediate waters. The simulation reproduces very well the mean salinity profile with its different water masses and its standard deviation. In more detail, the salinity of the intermediate waters is on average slightly underestimated in the Levantine basin (0.027 at 200 m) and overestimated in the Adriatic (0.055). The temperature profile is also well represented despite an overestimation between 400 and 600 m that produces a slight underestimation of density. The very characteristic shapes of the T/S diagrams over the 3 regions are very well represented (see for example the relatively less salty surface water in the Adriatic, more salty ones in the Levantine and Aegean (on this average because the variability is high for the latter, see below). In the Aegean, the minimum salinity located at 800 m in the observations (slightly deeper in the simulation) corresponds to Transitional Mediterranean Water (TMW) which is ancient water of the Eastern Mediterranean that replaced the dense waters formed during the EMT and exported to the deep basin (Velaoras et al., 2014). At 1000 m, the densest waters are in the Adriatic, but very dense waters also occupy the southern Aegean below this depth.

Fig. 8 presents the temporal evolution of the monthly averages of observed and simulated Argo salinities at 20, 225 and 800 m and temperature at 225 and 800 m. The depth of 225 m was chosen as a compromise between west and east in order to be as often as possible in intermediate waters (more details in section 4.2). The seasonal cycle is clearly visible on the salinity at 20 m with the maximum around October well phased in the simulation. At 225 m, the seasonal cycle is sometimes perceptible with a decrease in temperature and salinity around March also reproduced by the simulation. Despite trends cannot be drawn too roughly from these curves because of the variability of the spatial and temporal sampling, a trend towards increasing salinity at 225 m seems clear. The correlations are always significant (p-value$\ll$0.01) and strong (close to 0.9 except 0.73 for temperature at 800 m). The modeled and observed standard deviations are also similar.

To complete this analysis, Fig. 9 shows the observed and simulated mean salinity profiles for the four seasons and over the three formation areas. The Levantine basin has the highest seasonal variability over the first 150 m. This variability, which is well reproduced by the model, illustrates the dynamics of the salinity minimum marking the Atlantic waters, which deepens from 30 m in spring to 80 m in autumn, while in summer and autumn the saltier Levantine Surface Water occupies the first tens of metres. In winter, these two water masses are mixed. In the Adriatic, apart from the bias of the intermediate layers already noted (below 100 m depth), the seasonality of the stratification is also well reproduced by the model with, apart from winter, the low surface salinities linked to the fluvial inputs and the tendency to mix in winter. In the South Aegean, the model-observation agreement is less good in the

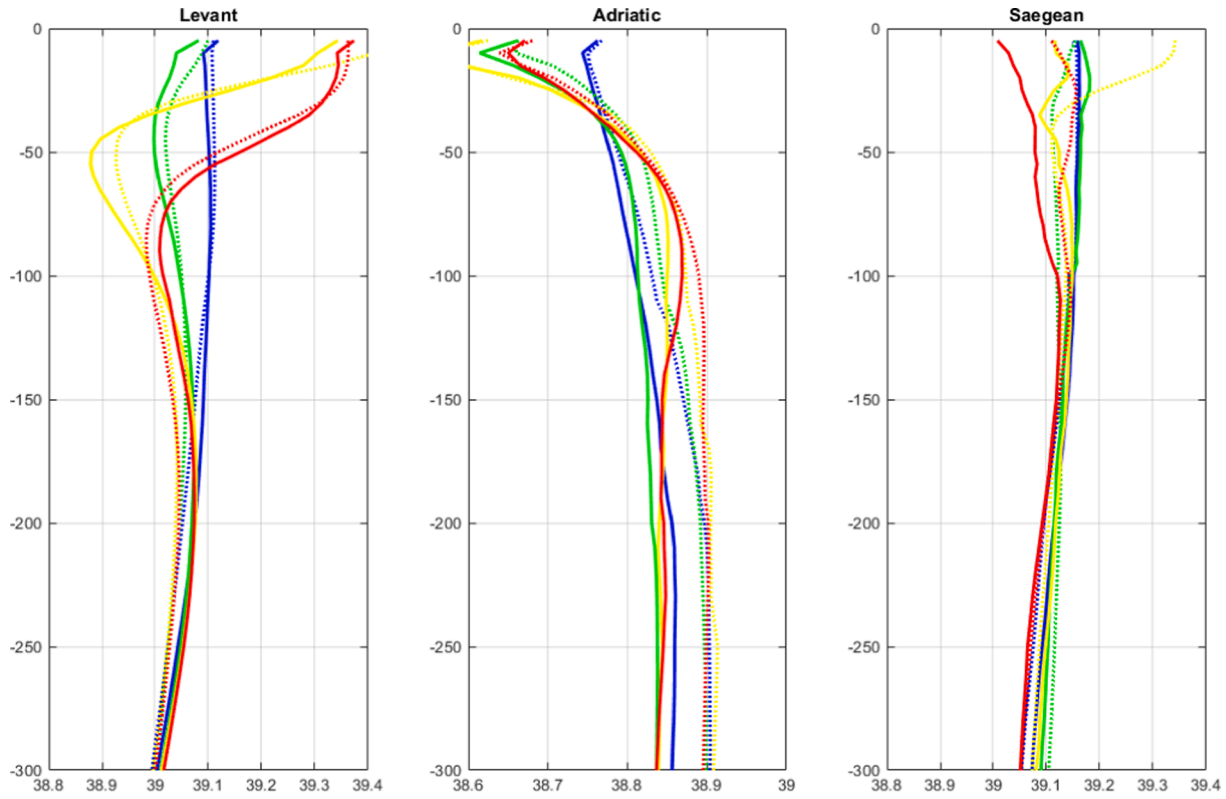

Fig. 9. Seasonal salinity profiles of the upper layer (300 m) in the Levantine (left), Adriatic (middle) and South Aegean (right). Winter (blue), spring (green), summer (yellow), fall (red). Solid lines are for observations, dotted lines for simulation.

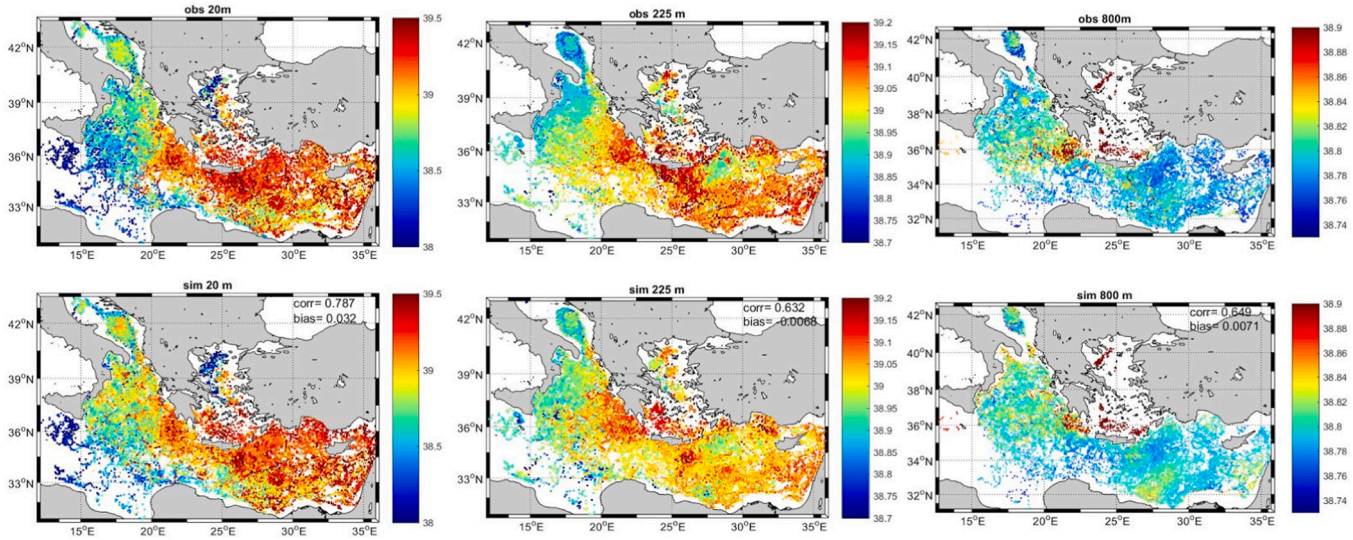

Fig. 10. Salinity observed (top) and simulated (bottom) at 20 m (left), 225 m (center) and 800 m (right) as noted in the figure. Each point corresponds to an observed / simulated Argo profile. The salinity range common to the observed and simulated values is adapted to each depth.

stratified period, while the winter profile is well represented. As pointed out above, spatial variability is important in this region. Moreover, the number of Argo profiles is relatively small, making the identification of a mean seasonal variability a difficult issue from the Argo database at the scale of this region.

Fig. 10 maps the observed and simulated Argo salinity at the three levels (20, 225 and 800 m), all times combined (temperature at 225 and 800 m is shown in Appendix B). The correlations and biases are now calculated from all 25,000 points and correspond rather to a spatial correlation insofar as the temporal variations are small compared to the spatial gradients. The spatial structures are correctly represented by the model as shown by these correlations which decrease with depth but remain strong. The mean biases are at most 3 hundredths consistent with Fig. 7. At 20 m, the major flaw is an overestimation of salinity in the Ionian. Looking more specifically at this zone, we see that the overestimation is located over a 2-year period starting in the summer of 2017, during which the observed salinity decreases, also imprinting the salinity curve of the whole basin over 2018 (Fig. 8). We have noted this problem in the various sensitivity tests we have carried out, but sometimes with a lesser intensity without any clear explanation for this

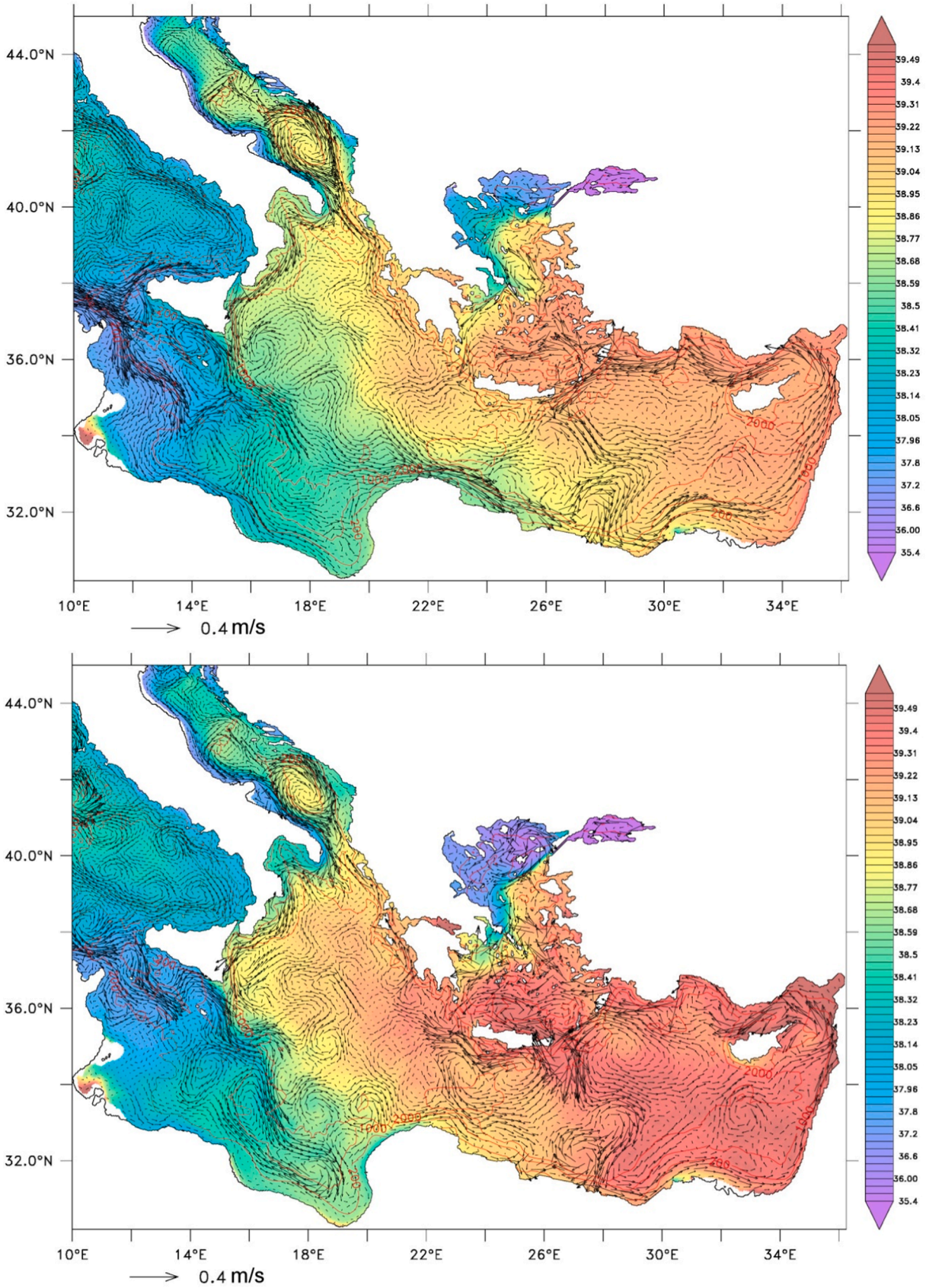

Fig. 11. Salinity and current simulated at 15 m depth and averaged over (top): January, February and March 2012 to 2019; (bottom): July, August and September 2012 to 2019.

sensitivity. This decrease in salinity, which corresponds to more intrusions of Atlantic Water in the Northern Ionian, is linked to temporary anticyclonic reversals of the Northern Ionian Gyre in 2017–2018 (Notarstefano et al., 2019). In the South Adriatic Pit, salinity increases from the periphery of the gyre towards the center, in observations and simulation. Along the African coast, the low-salinity of Atlantic Water is clearly visible along the Libyan coast but its signal is gradually weakening along the Egyptian coast. Further north, the simulation captures the strong salinity gradient between the western and eastern Ionian Sea. South-west of the Peloponnese, the Pelops anticyclonic salty eddy is clearly visible. It should be noted that anticyclonic eddies sometimes trap the floats for several months, which accentuates their footprint on the figures, while a positioning in space and time necessarily different in the simulation tends to dilute the signal and biases the comparison. Salinity is high in the northern and eastern parts of the Levantine basin. Different eddies clearly appear in the observations and the simulation, such as Ierapetra southeast of Crete and others located between 33 and 34°N from Libya to southern Cyprus. In the Aegean, the Black Sea Water path is very well reproduced in the north and along the northwest coast, while in the east, according to observations, salinity increases from north to south to reach its maximum in the Cretan Sea.

At 225 m, the salinity gradient remains strong between the west and east Ionian. In the Levantine basin, we find the weak underestimation mentioned above, and on the other hand the saltier signal of the anticyclones is well present. The Rhodes gyre that did not appear on the signal at 20 m depth is now clearly visible with relatively low salinities that mark the upwelling associated with cyclonic rotation. At the northern end of the Aegean, the Black Sea signal is no longer visible but it is clear in observations and simulation on the northwest coast.

At 800 m, one can still make out a weak signal of Pelops, Ierapetra and a band stretched northeastwards in front of Egypt at about 27°E, the latter overestimated in the simulation. This region corresponds, on the contrary to Pelops and Ierapetra, to rather low-salinity surface waters. At this depth, according to the T/S diagram of Fig. 7, the Aegean Sea is much saltier than the rest of the basin. Along the northwestern coast of the Ionian, the simulated salinity is too high, probably because it is impacted by the too strong salinity of the water flowing out of the Adriatic.

In conclusion, the bias of the simulation is low (a few hundredths). It reproduces globally well the spatial variations in temperature and salinity whether they are related to the path of the Atlantic, intermediate and Black Sea water masses. These water masses are well positioned vertically. The following section presents the surface and intermediate circulation.

4. Results and discussion

4.1. The circulation of surface water

a. Sicily Channel and Ionian

Fig. 11 shows the simulated salinity and mean circulation at 15 m depth (to avoid the Ekman component especially in summer) for winter and summer. In the first case, January, February and March were averaged, and the same for the second case with July, August and September, from 2012 to 2019.

In both cases, there is a cyclonic circulation around the basin but with substantial differences. The Atlantic Water enters the Sicily Channel along the north Tunisian coast. While in winter, part of the vein circulates cyclonically in the Tyrrhenian, in summer most of the water vein enters the eastern basin, which seems to be in line with the minimum transport observed at the Corsica Strait in summer as reported by Béranger et al. (2005). In the Central Mediterranean (Sicily Channel, Tunisian coast and western Libya), the path of Atlantic Water is in agreement with Sorgente et al. (2011) (their Fig. 2) and Menna et al. (2019b). In winter, the main vein follows the Tunisian slope up to about 13°E (with currents exceeding 35 cm/s in front of Cape Bon) and then splits into several branches, the main one being the Atlantic Tunisian Current (BATC) branch, which heads eastward around 34.5°N. Another branch follows the coast and corresponds to the Atlantic Libyan Current (ALC). In the South Ionian, these different branches meet near Benghazi on the Cyrenaic coast. In summer, according to Gerin et al. (2009) and Sorgente et al. (2011), the Atlantic Water mainly follows the Atlantic Ionian Stream (AIS) along the southern coast of Sicily, bypassing the Adventure Bank and sticking again the coast at about 14°E with velocities of about 25 cm/s. One difference with Sorgente et al. (2011) is that at the southeast corner of Sicily, the vein does not turn north which, probably in our case, would correspond to cyclonic conditions of the North Ionian Gyre as attested by Gačić et al. (2014), since the last inversion in 2011. Between 15 and 19°E, the current (of the order of 15 cm/s) describes an elongated anticyclonic loop which seems to correspond to the anticyclonic zone of the Mean Dynamic Topography (MDT) of Rio et al. (2007) (their Fig. 11) and to the extended Sidra Gyre of Menna et al. (2019b) (their Fig. 2b). Gerin et al. (2009) also described from drifters trajectories a large anticyclonic loop between 14 and 17°E. They attributed it to the anticyclonic rotation of the wind from northwest to southwest that characterizes this region in summer (see Fig. 3b of Gerin et al., (2009)). Further north, east of 17°E, unlike in winter, the Atlantic Water does not reach the Benghazi region as a vein but rather as a train of anticyclonic eddies about 80 km in diameter. The simulation also reproduces the cyclonic structures, Adventure Bank Vortex (ABV), Messina Rise Vortex (MRV) mainly in summer here, and incorporated in the large basin-wide cyclonic gyre as stated by Menna et al. (2019b), Libyan Shelf Break Vortex (LSBV) - refer to Sorgente et al. (2011) for details - and anticyclonic ones, a number of which on these averaged fields resemble meanders rather than closed eddies.

In summer and winter, north of the Ionian, the circulation is alongslope cyclonic with a current that is wider in winter than in summer along the east coast, flowing west of the Ionian archipelago while in summer the current accelerates (~15 cm/s) between the Peloponnese and the islands of Zakynthos (Zante) and Kefalonia. Along the western Ionian coast, reinforced by the surface water flowing out of the Adriatic, the current forms a rapid (20 cm/s), narrow and stable vein which, according to Millot and Taupier-Letage (2005), joins at the southeast corner of Sicily (or a little further south in winter) the main Atlantic Water vein coming from the western basin. The vein formed by this convergence is thus composed of water older and saltier in the north than in the south. It can be seen from the surface temperature (e.g. Fig. 6 bottom right) that the two veins are separated by the Maltese filament, formed by cold water upwelled off southwestern Sicily and which is advected towards the southeast (Millot and Taupier-Letage, 2005; Hamad et al., 2006). In the center of the Ionian basin, in both seasons, there are a large number of eddies, most often anticyclonic. To the east (36°N, 22°E), Pelops is the saltiest.

b. Levantine basin

Starting from Cyrenaic, there is a cyclonic alongslope current around the Levantine basin in both seasons. This current (corresponding to the Libyo-Egyptian Current to the south) is more intense and more stable in winter exceeding 35 cm/s between 22 and 23°E. The instabilities generate anticyclonic meanders and eddies that mark the average circulation in summer up to 28°E. At 27°E, in the Herodotus Trough, a northeastwardly stretched anticyclonic structure (fed by eddies that detach from the coast) is found in both seasons, corresponding to the Mersa-Matruh Eddies (or Herodotus Trough Eddies or the SLw of Millot and Taupier-Letage (2005) described above). Further east, the increase in salinity seems to be linked to the convergence of the alongslope current with a current coming from the north, partially closing the cyclonic loop of the eastern Levantine sub-basin. This current connects the western branch of the Rhodes Gyre and the eastern edge of the Mersa-Matruh anticyclonic structure. From 29°E and all along the Middle East coast (up to 34°N), the current is much more stable in agreement with Millot and Taupier-Letage (2005). In summer, the shallower current flows along the coast while in winter it flows above

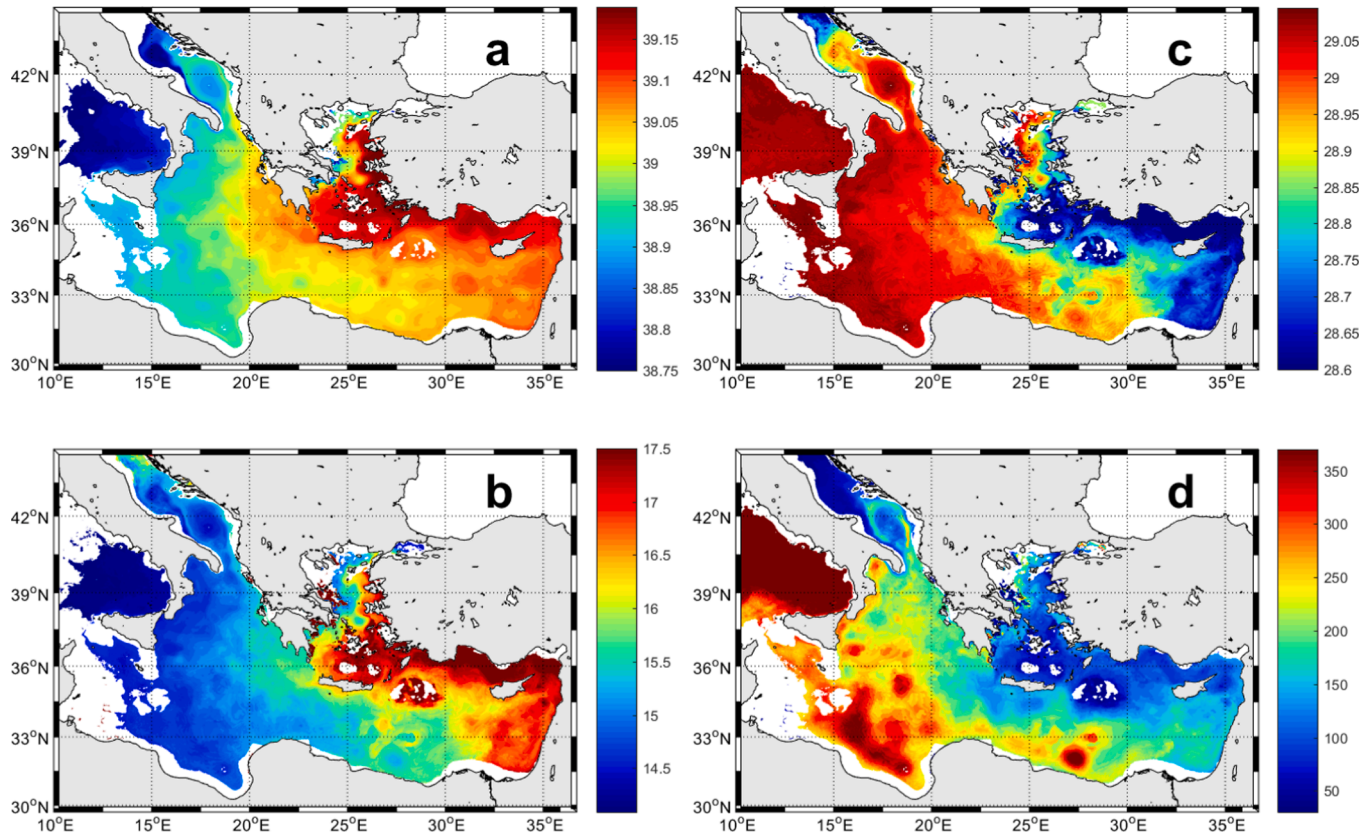

Fig. 12. Characterization of intermediate waters in summer. a: maximum subsurface salinity, b: temperature and c: potential density anomaly at the same level as a, d: depth of this maximum salinity. No subsurface maximum is found in white areas.

the 1000 m isobath. Offshore, the Cyprus Eddy is on average present summer and winter over the Eratosthenes Seamount, with a diameter of about 130 km. Between Cyprus and the Syrian coast, in summer, the cyclonic Latakia eddy (Ozsoy et al., 1993; Menna et al., 2012) is fed by a branch of current flowing eastward at 34°N, closing a vast cyclonic gyre merging the Rhodes gyre and the basin surrounding Cyprus. This branch could correspond to the Mid-Mediterranean Jet of Robinson and Golnaraghi (1993). However our simulation does not show a single, coherent stream, but rather a path defined by the western edge of Mersa-Matruh Eddies continued with the southern branch of the cyclonic gyre.

In the north, the Asia Minor Current is strong in winter (30 cm/s) and forms long wavelength meanders induced by the topography while it is weaker and diffuse in summer. This current splits into a vein which enters the Aegean through the Rhodes and Karpathos Straits in winter and a vein which constitutes the northern branch of the Rhodes Gyre. The Rhodes Gyre itself contains in both seasons secondary cyclones of smaller size in winter (~60 km) than in summer. As already mentioned, further west, Ierapetra is powerful at the surface in summer and is also closer to Crete. Its elongated shape towards the south indicates a recurrent displacement in this direction as indicated by Mkhinini et al. (2014). Its mean diameter (estimated in west-east direction) is about 100 km, in the high range of typical values given by Ioannou et al. (2017) and the current reaches there an average of 35 cm/s close to the values of 40 cm/s measured by ADCP (Ioannou et al., 2019). It is interesting to note that in summer, the current along its eastern branch is intensified above 40 cm/s. This west east asymmetry is due to the convergence of two currents that tighten the front east of Ierapetra, the first is the rim current of the Rhodes Gyre which flows from the north-east and the second is a current that enters from the Aegean through the Kasos Strait and is partly fed by the branches coming from the Rhodes and Karpathos straits which form a cyclonic circulation in the Aegean leaning against the Cretan Arc. The current that enters through the Kasos Strait seems to be, in addition to the direct effect of the wind curl, a source of energy for Ierapetra. This general behaviour is in agreement with Kontoyiannis et al. (1999) who noted in summer a complex interaction between the cyclonic gyre localized north of Crete, Ierapetra, and the westward extension of the Rhodes Gyre producing a net flow from the Aegean to the Levantine in the Kasos Strait. Finally west of Ierapetra, a large cyclonic zone is simulated, extending further west in winter with a west-east extent of about 400 km, sustaining a strong current to the north in summer (25 cm/s) transporting water flowing around the outer edge of Ierapetra. The wide cyclonic summer structure is clearly formed by two cyclonic eddies. It is known as West Cretan Gyre (Hamad et al., 2005) or Cretan Cyclone (Malanotte-Rizzoli et al., 1997). The surface circulation simulated here is close to the scheme of Malanotte-Rizzoli et al. (1997) (their Figure 24a) which shows the Levantine Surface Water flowing between Crete and the Cretan Cyclone, which then turns partly southward around the cyclone, and for another part is driven anti-cyclonically around the Pelops gyre. The third branch of Malanotte-Rizzoli which enters the Cretan Sea is not present here.

c. Aegean Sea

We do not claim that the topographic complexity of the Aegean Sea is represented correctly by our grid (for example, the island of Evoia is connected to the continent to the northwest). We therefore focus here on the main features of the circulation. The surface salinity in the Aegean Sea shows three zones: (1) the north and west influenced by the low-salinity Black Sea Water, (2) to the east, high-salinity influenced by the Levantine Surface Water but also in summer subject to upwelling (e.g. Fig. 6) induced by the Etesians, and (3) to the south, the cyclonic Cretan Sea with high salinity. The seasonal variability of salinity in the north is primarily induced by the seasonality of the Black Sea Water transport, strong in summer, and also by low vertical mixing at this season. In agreement with Zervakis and Georgopoulos (2002), the front separating the Black Sea Water and the Levantine Surface Water is

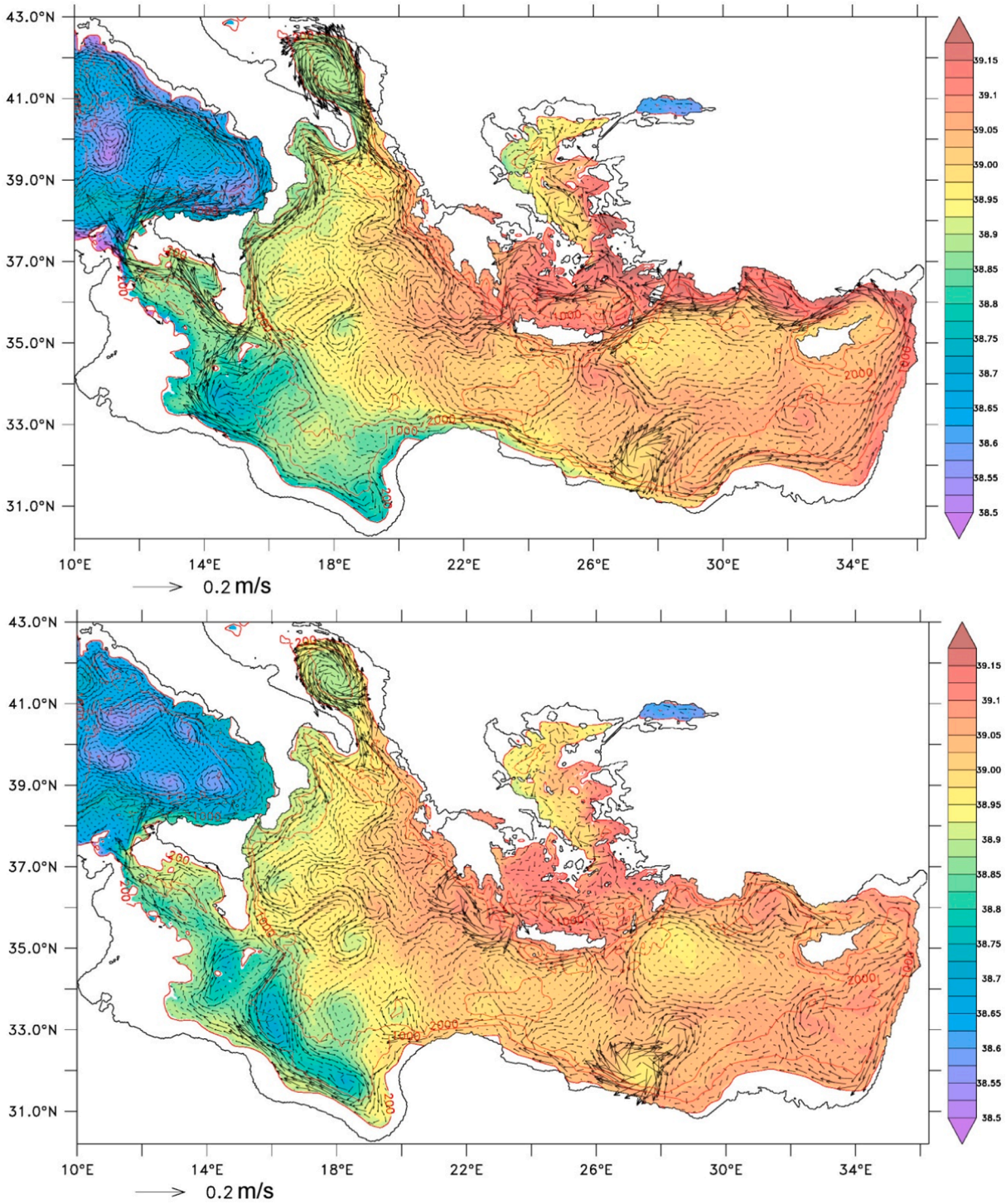

Fig. 13. Salinity and current simulated at 225 m depth and averaged over (top): January, February and March 2012 to 2019; (bottom): July, August and September 2012 to 2019.

narrow in summer and positioned south of Lemnos while in winter it is more diffuse and spreaded on both sides of the island. To the northeast and more clearly in summer, the Samothraki anticyclone, considered by Nittis and Perivoliotis (2002) as a permanent structure is present. To the northwest, the circulation in the Sporades basin is cyclonic in winter and anticyclonic in summer, the latter characteristic is not, to our knowledge, present in the literature, although it is mentioned by Kontoyiannis et al. (2003) for the subsurface from a campaign carried out in September 1998. Further south, between Evoia and Chios (38.5°N, 25°E), the Chios cyclone (Gerin et al., 2014), one place where the densest water masses in the Aegean Sea are formed through open ocean and shelf convection processes (Vervatis et al., 2014) appears as a structure elongated in the south-north direction. In summer, south of Athens, an anticyclone with Black Sea Water well diluted at this latitude and possibly wind-induced is clear. The Cretan Sea is globally marked by a cyclonic circulation well delimited in the north in winter by a powerful current flowing from the Levantine. It is composed of one or two gyres which extend between the two branches of the Cretan Arc. The simulation corresponds well to what was observed by Theocharis et al (1993) for the 1986 winter. On the other hand, we do not obtain an anticyclonic

circulation in northwest Crete as reported by Theocharis et al. (1999) in summer 1994 (associated with an intrusion of low-salinity Atlantic Water) and winter 1995.

d. Adriatic Sea

The simulation shows the main characteristics of the circulation in the Adriatic, namely the cyclonic circulation formed from the Eastern Adriatic Current following the east coast to the Istrian Peninsula and the Western Adriatic Current following the west coast. This circulation encompasses three cells in the sub-basins of the South Adriatic Pit, the Jabuka Pit in the center, and the north (Poulain, 2001), the first two forced by bathymetric lows. The strongest currents are around the South Adriatic Pit with intensities of 20 to 25 cm/s, a little wider in summer and a little stronger in winter with maximums along both the west and east coasts and particularly in winter in front of the Albanian coast (>30 cm/s). On a smaller scale, in summer, an anticyclonic circulation north of 44°N near the Istrian Peninsula shown by Krajcar (2003) from the analysis of historical data as an extension of an anticyclonic meander from the Po Delta is represented. Krajcar (2003) also shows the presence of another anticyclone further south near 43.7°N, 15°E also visible in the simulation in summer. Finally, the extreme north of the Adriatic (north of 45°N) is occupied by a cyclone that extends between the west and east coasts (not shown).

4.2. Intermediate water circulation (LIW/CIW)

The average characteristics of the intermediate waters (salinity, temperature, potential density and depth) were calculated from the average of summers fields (July to September) 2012 to 2019 (Fig. 12). At each grid point, the local maximums of the salinity profile (a point surrounded by two lower values) are searched for and the largest maximum is selected. The white areas correspond to the points where no local maximum exists (salinity increase or decrease from the bottom to the surface). Summer was chosen because this season minimizes the number of these points which, outside the shallow regions, concern a few points in the Rhodes gyre and the South Aegean. In the northern Levantine Basin, the characteristics of the LIW are far from uniform. In the center of the Rhodes Gyre, the salinity maximum is very shallow (40–70 m) with salinities between 39.07 and 39.09 (at this depth, the temperature is very variable and affected by summer warming). In the Asia Minor Current, typical values are (39.11, 16.9 °C) and maximum values are located in front of Antalya Bay around (39.17, 17.5 °C), in both cases at about 100 m depth. In the South Aegean we find values close to the latter, but rather at 70–80 m depth. Moving south and west across the basin, the temperature and salinity decrease very rapidly and the potential density increases.

These patterns give indications of preferential transport pathways that will be detailed later. The potential density anomaly, which was around 28.7 in the areas detailed above, increases rapidly in the Ionian with values of 29 along the eastern Ionian coast, then a strong increase again along the western Ionian coast around 29.07 to finish around 29.08 in the Sicily Channel and in the Southern Ionian. These increases in density are accompanied by increases in intermediate water depth, about 200 m for the eastern Ionian, 230 m for the western Ionian, 270 m for the Sicilian Channel (with strong spatial variabilities related to the mesoscale).

The depth of 225 m was chosen to present the intermediate circulation (Fig. 13) knowing that the intermediate water layer is thick and the current is not very sensitive (less than salinity) to a variation of 50 m. Outside the Sicily Channel and the South Ionian, in winter, the main features of the circulation are little different from the surface circulation but with weaker currents, by about a factor of 2. In the Levantine basin, the Rhodes Gyre must be considered specifically because, although it is certainly the primary site of LIW formation, it is not characterized by high salinities at this depth. Indeed, it is a cyclonic zone with a density dome where the maximum salinity is above 70 m depth. The depth considered here is therefore populated with water denser than LIW. The southern edge of the gyre is characterized by a maximum salinity which corresponds to water subducted from the gyre and transported cyclonically around it. In the north, the Asia Minor Current is saltier in winter than the other regions of the Levantine basin and also saltier than in summer. Indeed, the winter mixed layer whose depth is here about 100–125 m has incorporated first, Levantine Surface Water, whose salinity increased continuously in summer and until November under the effect of evaporation, and second, subsurface Atlantic Water relatively salty because of the large distance from Gibraltar. In late winter / early spring, the surface is, thanks to the powerful cyclonic circulation that takes place in winter, covered with less salty Atlantic Water that isolates the salty water at depth. This “local” mechanism of intermediate water formation, different from that of the Rhodes Gyre whose water formed becomes intermediate at its periphery during subduction, is the cause of the seasonal cycle of salinity observed here. The current is clearly less marked in summer than in winter (>20 cm/s at 150 m in winter and about 10 cm/s in summer), and also further from the coast, looking more like a rim current of the Rhodes Gyre, giving the possibility for the development of anticyclones linked to the topography in the Gulf of Antalya and between Rhodes and Turkey. These anticyclones temporarily trap a fraction of the intermediate water formed in winter while the westward mean circulation advects part of the water formed, out of the formation area. South-east of the Levantine Basin in summer, we notice that the current noted at the surface, northward, narrow and stuck to the coast, reverses in depth. Associated with other structures such as the Cyprus Eddy, it forms a large anticyclonic structure reminiscent of the pattern of Robinson and Golnaraghi (1993) (Fig. 1a), but here, present only in summer and subsurface. Like all other anticyclonic structures, it downwells salt at depth. Katz et al. (2020) noted off Haifa a strong slowing in summer of the 30–200 m averaged current above the 1500 m isobath, which is verified by our results but their observation site is too far offshore to detect a possible reversal of the current direction as represented by our simulation.

On a larger scale, the circulation of LIW in the Levantine in winter seems confined in its eastern part, east of 26°E. Indeed, the westward current under Crete is less powerful than in summer and seems rather related to the vast cyclonic structure that encompasses the Cretan Cyclone. Surprisingly, contrary to what has been seen at the surface, the Ierapetra anticyclone at intermediate depths is larger in winter than in summer, more salty and also detached from the coast towards the south. During this season, it is regularly subjected to advections of surface Atlantic Water from the south of the basin which mask it, while at greater depths, the downwelling of the salty surface waters of summer and autumn continues. Ierapetra certainly plays an important role in the bifurcation of the LIW towards the south at the corner of Crete while the Mersa-Matruh Eddies play the same role in the south of the basin to redirect the LIW towards the east. In summer, on the other hand, it seems that the more northern position of Ierapetra and the weaker current that characterizes it at depth favors the bifurcation of the LIW towards the west under Crete. Spring (not shown) is the most favorable season for the advection of the LIW to the west as Ierapetra is weak or non-existent, the Rhodes gyre is destructured on its western flank allowing the current bounding the Rhodes gyre along the Cretan Arc to extend under Crete.

From spring to autumn, the LIW mainly escapes from the Levantine under Crete. In winter, on the other hand, it flows into the Aegean (see also section 4.4) through the straits of the East Cretan Arc and follows the same paths as at the surface. Two branches with different characteristics can be distinguished. The first branch, saltier, corresponds to the water formed in the northeast of the basin, transported by the Asia Minor Current introducing into the Aegean between Rhodes and Turkey and then flowing along the Turkish coast. The second branch, less salty formed in the Rhodes Gyre exits through the Karpathos and Kasos Straits and circulates cyclonically around the Cretan Sea.

At its exit in the Ionian, intermediate water (LIW/CIW) produces several branches, first of all, as for the surface water, alongslope

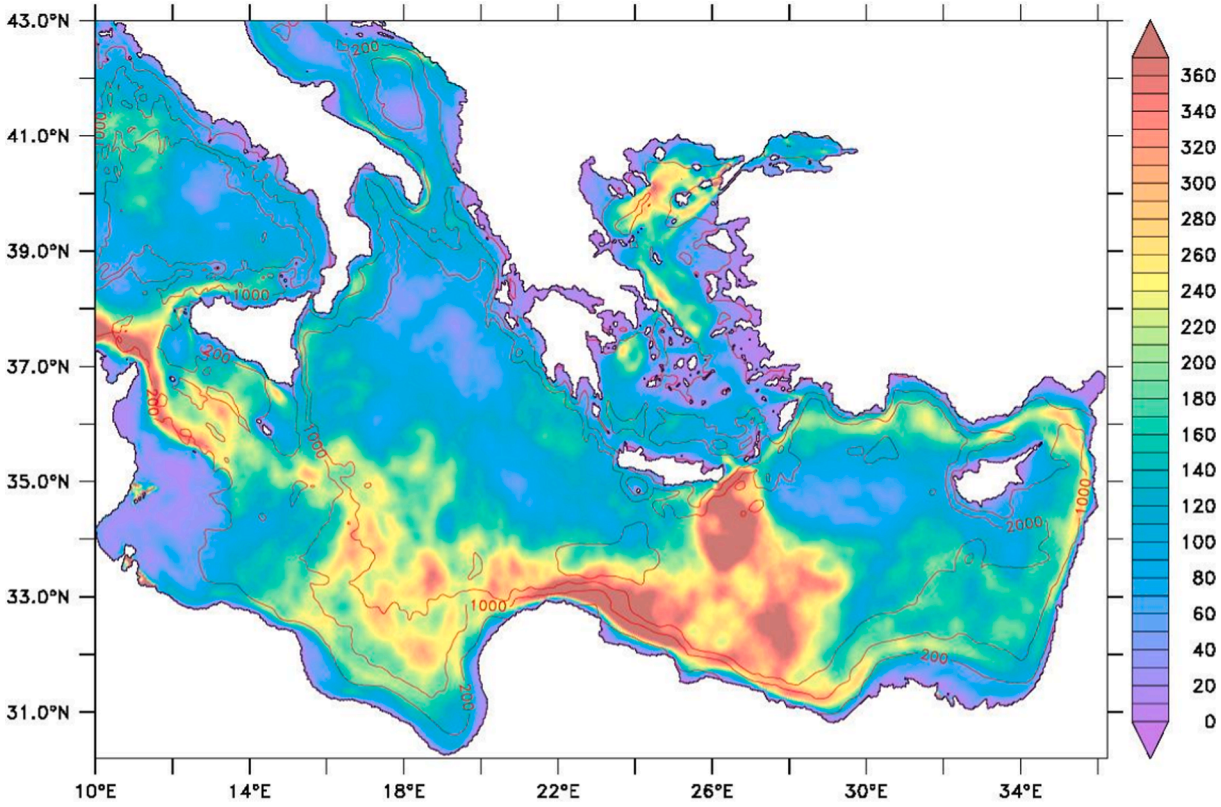

Fig. 14. Surface geostrophic eddy kinetic energy (cm^2/s^2) averaged over 2012–2019.

northward along the Ionian east coast. The main branch turns around Pelops and divides on the one hand by recirculating southward around the Cretan Cyclone and on the other hand by producing branches flowing northward and westward producing meanders and eddies. These branches clearly accelerate the dispersion of salt in the center of the Ionian, which results in a significant difference in salinity between the eastern and western Ionian coasts (Fig. 12), a difference to which the Adriatic also contributes. From spring to autumn, as we have seen previously, the LIW flows along southern Crete, then turns around a powerful anticyclone that blocks the straits of the western Cretan Arc (Kithira and Antikithira) and redirects more efficiently than in winter, part of the intermediate water towards the west and the Sicily Channel while the other part recirculates towards the north around Pelops.

An important part of the intermediate water enters the Sicily Channel through the opening located at about 35°N while another part recirculates cyclonically towards the Levantine in winter, and towards the Gulf of Sirte south of the Ionian especially in summer. In this sub-basin, the core of the Levantine waters is located around 300–350 m thus below the depth shown in Fig. 13, which explains the low salinities of this figure, which correspond to the downwelling of the surface waters by the anticyclonic structures. However, the currents in Fig. 13 are still representative of the intermediate water showing an alongslope vein directed northwestward. In summer, this current is stronger and is intensified by the surface anticyclonic structure. In this season, this vein mainly reaches the main opening of the Sicily Channel (this is clearer at 300 m than in the figure at 225 m). In winter, on the other hand, the current rather penetrates through the complex topography of the southern half of the Sicily Channel to reach west of Malta the main vein flowing from the North Ionian. To our knowledge, this southern region is poorly documented, which does not allow us to verify our results. In the Sicily Channel, the current is much stronger in winter than in summer according to observations of stronger transport in the Sicily Strait in winter (Manzella et al., 1988; Béranger et al., 2004) and is at this season mainly stuck to the Italian side. It should be noted that just above the sill we find maximum salinity around 300 m depth with slightly deeper maximum velocities of 25 cm/s in winter and 12 cm/s in summer (not shown).

4.3. Circulation variability

The eddy kinetic energy (EKE) is used to quantify the variability of surface circulation. It provides information on the variability of the general circulation (mainly alongslope currents) and, more in the center of the basins, of the mesoscale activity. Fig. 14 shows the average over 2012–2019 of the surface geostrophic EKE:

$$\overline{EKE} = \frac{1}{2}\left(\overline{\left(Ug - \overline{Ug}\right)^2 + \left(Vg - \overline{Vg}\right)^2}\right)$$

where U_g and V_g are the components of the surface geostrophic current calculated from the gradient of the surface elevation of the model averaged over 24 h. The averaging operators correspond to 8-year time averages.

The high values are concentrated in the Sicily Channel, in the south of the Ionian, the Cyrenaic and Egyptian coasts up to the Nile delta. The areas of strong EKE aligned with the isobaths are related to the seasonal variability of currents identified previously (see Fig. 11 showing the strong/weak winter/summer currents in the Sicily Channel, along the Cyrenaic coast and in the Asia Minor Current). In the Aegean, the strong EKE patterns correspond to the variability of the Black Sea Water path.

Offshore, the EKE allows to identify the most energetic eddy zones such as the South Ionian around the 1000 m isobath, or the Cretan Passage with the instabilities of the Libyo-Egyptian Current and of the Mersa-Matruh Eddies in the south, and of Ierapetra in the north. All these structures are also present and dominant in the study of Pascual et al. (2007). On the other hand, the latter shows an intense zone in the southeast of the basin, the so-called Shikmona zone, which is calmer in our simulation.

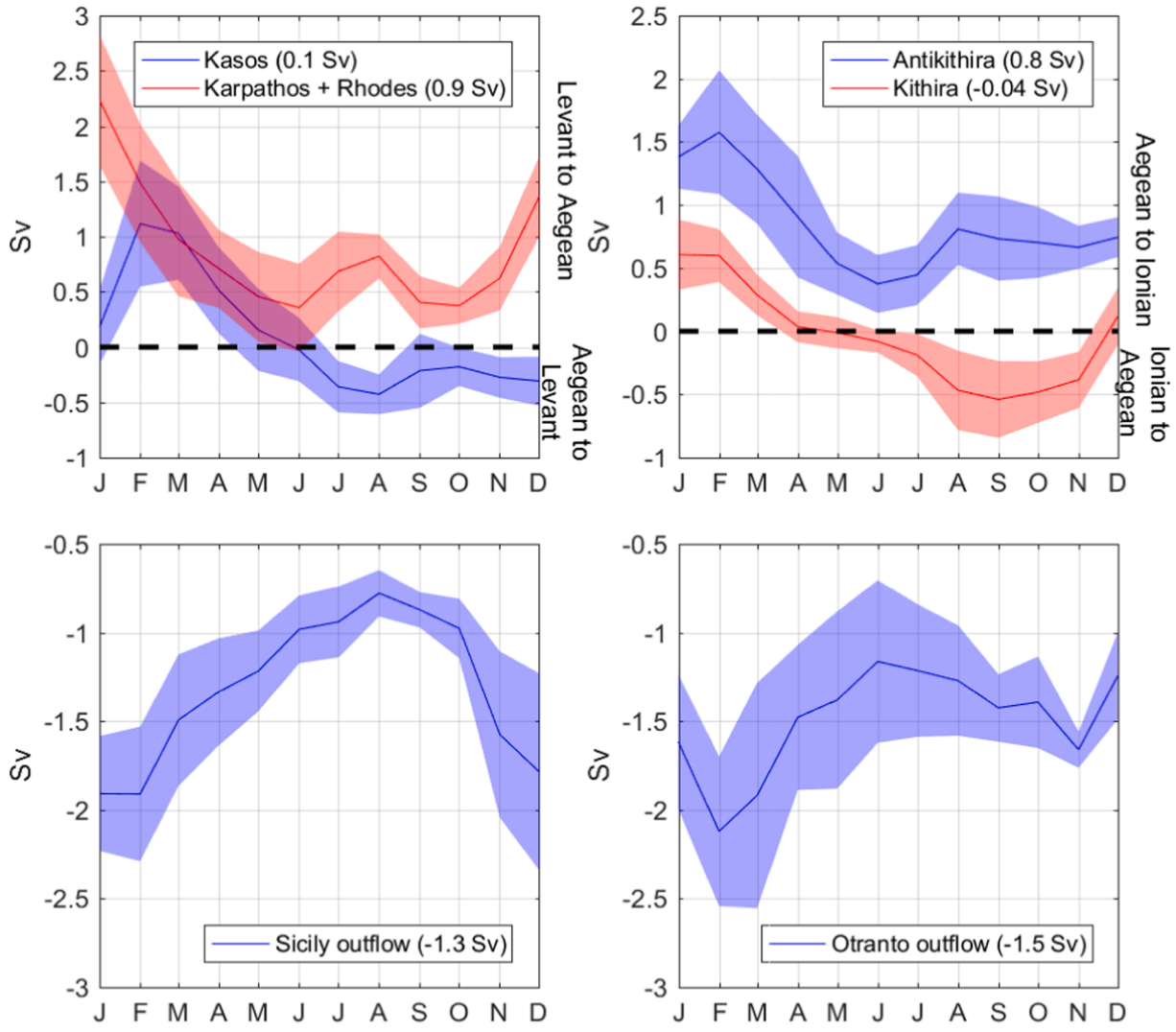

Fig. 15. Monthly climatology (and standard deviation) of transports in the straits. (top) between 0 and 400 m for the Cretan Arc with on the left: the eastern straits between Levantine and Aegean (Karpathos and Rhodes were grouped together), on the right: the western straits between Aegean and Ionian. The sign convention (positive = cyclonic direction) is shown in the figure. (bottom) outflow at the Sicily Strait on the left and Otranto Strait on the right. The annual average transports are in the figure.

The regions of lower EKE are the continental shelves and cyclonic gyres (Rhodes and the South Adriatic) in agreement with the results of Pascual et al. (2007) calculated over 9 months with multisatellite altimeter missions.

Furthermore, the surface circulation (Fig. 11), although a seasonal average over 8 years, shows a large number of eddies in the Ionian, suggesting a strong recurrence of these structures present for some of them on both the winter and summer averages. This is the case, for example, of a group of 4 anticyclones with a diameter of 100 km and characteristic currents of 10 to 20 cm/s depending on the year, i.e. moderately energetic, 2 are located just north of the current flowing along the slope to the south-east of Sicily (about 36.5°N 16.3°E and 35.5°N 18.5°E) and the other two closer to each other around 37°N 18°E. The presence of each of these eddies varies from 4 to 7 summers out of 8. Another example, further north-east, is an anticyclone located around 37.7°N 19°E and neighboring a cyclone a little further south. All these eddies also affect the intermediate waters. The reasons for the recurrent presence of these eddies remain to be elucidated as well as their impact on the mean circulation of water masses and more locally on their retention and sinking. Indeed, it can be noted in Fig. 10 that the observed and simulated salinity at 800 m indicates a band of higher salinity around 36°N, 16-22°E, that would correspond to a downwelling of intermediate water related to the cumulative effect of the anticyclonic eddies.

4.4. Transport at straits

To complete this description, Fig. 15 presents the monthly transport climatology in the straits (shown in Fig. 2) calculated from the model results for 2012–2019. The straits of the Cretan Arc, unlike the Sicily and Otranto Straits, do not have an inflow/outflow of surface/deep water. Schematically, the inflow to the Aegean is through the eastern straits and the outflow to the Ionian through the western straits. Following Kontoyiannis et al. (1999), we have integrated the transport between the surface and 400 m as at greater depths, the dense Cretan waters (CDW), not considered here, dominate the outflow. Finally, for the sake of simplification, the Karpathos and Rhodes Straits have been grouped together because they function similarly.

The Kasos Strait, unlike Karpathos and Rhodes, has an inverted functioning in winter and summer with an inflow in winter toward the Aegean like Karpathos and Rhodes, and an outflow in the second part of the year. In winter, the transport, addition of the 3 straits, each about 50 km wide, exceeds 2 Sv. In summer, the symmetry of the two curves indicates, as observed above, that the flow entering the Aegean to the east

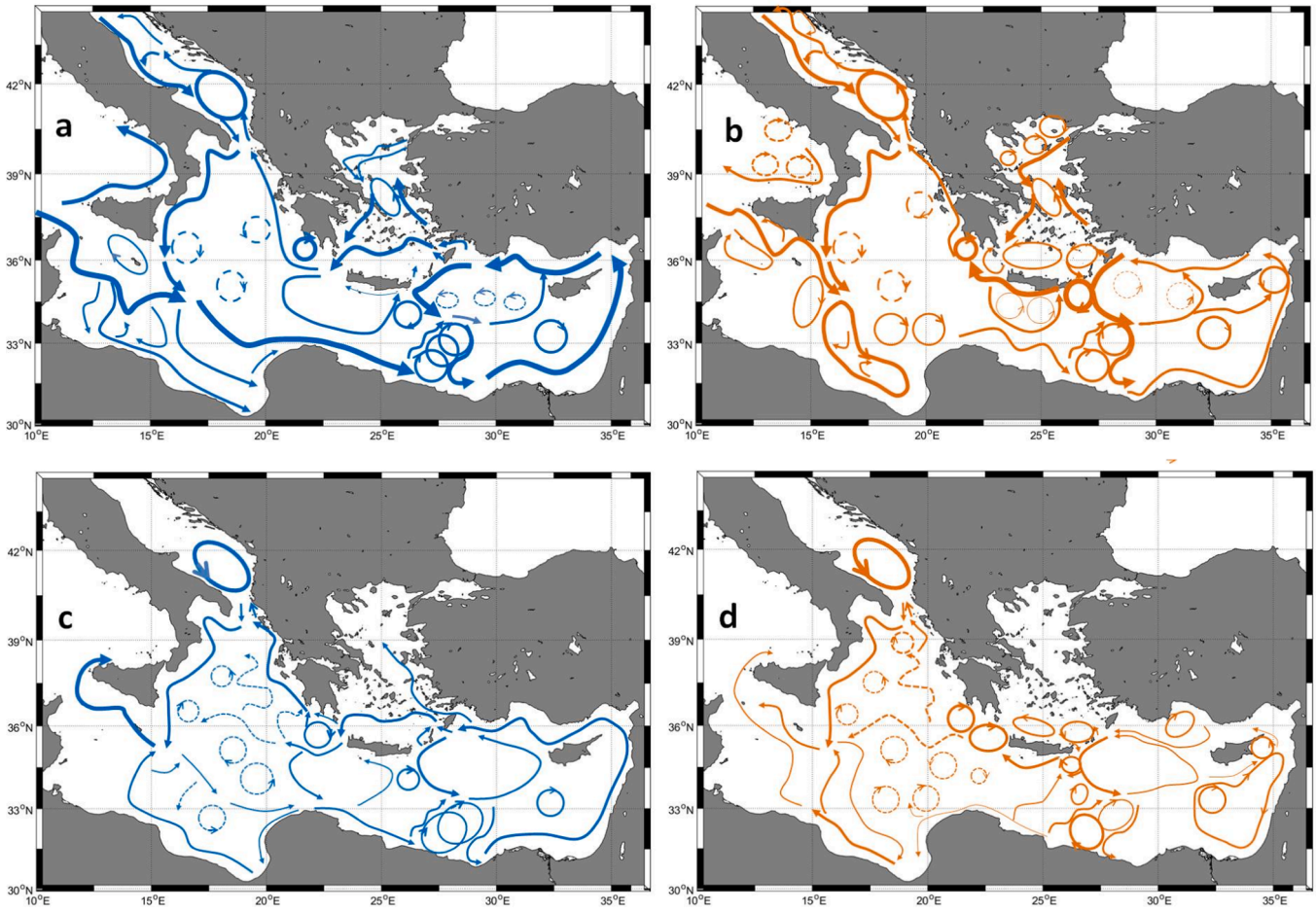

Fig. 16. Seasonal circulation of surface water (top, a and b) and intermediate water (bottom, c and d) inferred from the simulation. In blue, a and c are for winter, and in orange, b and d for summer.

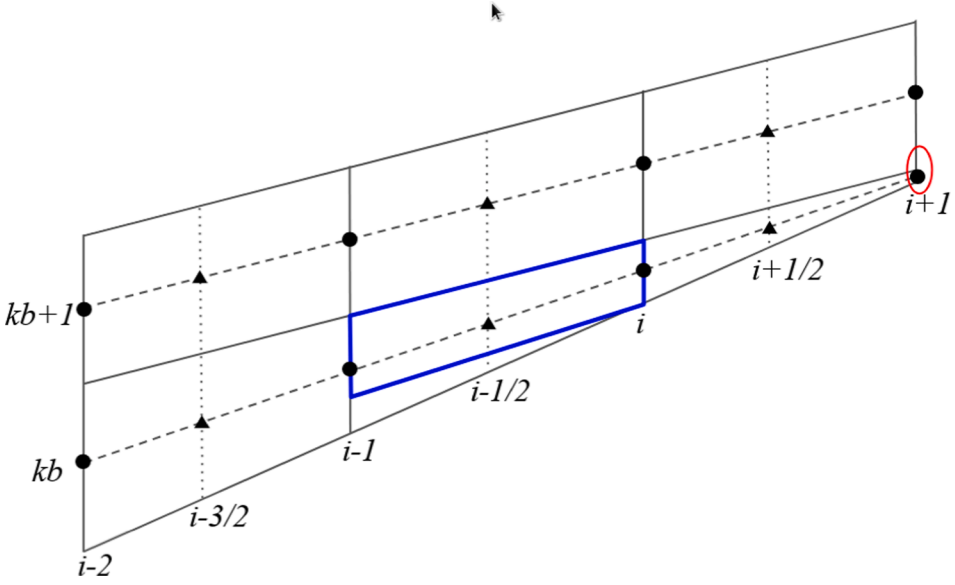

Fig. A1. First vertical levels above the bottom. The sloping solid black lines represent the upper and lower limits of the cells. The lower one represents the bathymetry. The vertical distance between two successive lines defines Δz, the thickness of the layers. The sloping dashed black lines represent the computational levels for tracers and velocities. The vertical solid black lines correspond to the integer indices i-2,i-1,…. … where the tracers are calculated and the vertical dotted black lines correspond to the half integer indices i-1/2,i + 1/2,.. where the velocities are calculated. The thick blue line corresponds to the boundaries of the sub-cell, corresponding to the calculation of the PGF at point (i-1/2,kb). The red circle designates a grid point where the cell thickness is small compared to neighbouring points ($\Delta z_{i+1/2}/\Delta z_i \gg 1$), raising a stability issue for the advection calculation. The black circles represent the calculation points of the tracers, the black triangles those of the velocities.

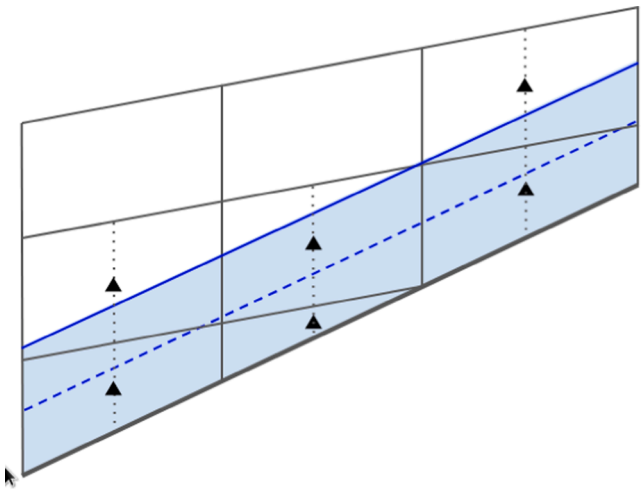

Fig. A2. Regular "virtual" bottom layer (in light blue). The solid blue line represents its upper facet and the dotted blue line its centre, where the drag coefficient and the bottom current are estimated. The solid black lines delimit the velocity grid cells. The black triangles correspond to the velocity points. The vertical dotted black lines indicate the two levels involved in the weighted average of the current for the calculation of the bottom friction. Note that the thickness of the virtual layer is equivalent to that of the second level above the bottom.

partially exits through Kasos after a cyclonic circulation. The order of magnitude found by Kontoyiannis et al. (1999) in 1994–1995 in Kasos of 0.7 Sv inflow in winter and 0.5 Sv outflow in summer is fully respected, whereas we do not find their summer inflow of 1.7–2.1 Sv by Rhodes and Karpathos.

West of Crete we find a symmetric functioning with a winter outflow of 2 Sv through the Antikithira and Kithira Straits (both about 30 km wide). In summer and autumn, we find a symmetry of the flows in these 2 straits with an outflow in Antikithira and an inflow in Kithira which reflects the presence of the anticyclonic eddy in front of the straits on the Ionian side. Our estimate for the winter outflow to the west corresponds to that measured by Kontoyiannis et al. (1999) but the summer outflow is underestimated (0.3 Sv compared to 0.8 Sv). The net transport through all the straits of the Cretan Arc is thus maximum between January and March with a gain of 0.4 Sv for the Aegean and is close to 0 in summer (annual average of 0.17 Sv). This net water gain between 0 and 400 m in winter is compensated by a dense water outflow under 400 m depth.

In the Sicily Strait, we obtain an average annual outflow of 1.3 Sv with a standard deviation of 0.14 Sv, higher than the value of 1.1 Sv of Astraldi et al. (1999) and 1.2 Sv of Bethoux (1980). The seasonality with the minimum in summer and the maximum in winter corresponds to the model and observation results presented by Béranger et al. (2004). Net transport over the whole water column is close to 0.02 Sv. In the Strait of Otranto, the annual outflow is 1.5 Sv (standard deviation 0.24 Sv) presenting a minimum in summer and a maximum in winter. Yari et al. (2012) gave an estimate of 1 Sv for 1994–1995 and Mantziafou and Lascaratos (2004) a mean value of 1.6 Sv with a model. However, Manca et al. 2002 noted that water flux in Otranto strait varies from year to year as a function of the intensity of the Adriatic dense water formation while Yari et al. (2012) claimed that their estimate should be considered as a lower limit value since, in that period, the Adriatic was producing relatively small quantities of deep water. As such, our period of simulation corresponds to intense formation in the Adriatic (Kassis and Korres, 2020) which could justify our stronger numbers. Finally, these different studies show a variable seasonality which is attested by our estimate. To close the budget, we find in the Messina Strait, an outflow of 0.07 Sv and a net transport of about 0.01 Sv, the first one negligible compared to the Sicily Strait, the other one of the same order of magnitude.

5. Conclusion

The 9-year simulation presented in this paper has been compared to surface observations (SST), and from 20 to 800 m, to the huge Argo database which counts over this period about 25,000 profiles in the Eastern Mediterranean. Generally the biases are low and the correlations are good over the salinity and temperature fields at different depths while the mean vertical profiles in each water mass formation sub-basin are also well represented. To our knowledge, this is the first time a model has been evaluated in such detail. The horizontal resolution of 3–4 km, and probably also a wind with relatively high horizontal resolution, make it possible to represent the mesoscale as attested by the recurrent and faithful representation of many eddies well identified in the literature as well as fine SST structures.

This paper has focused on the circulation of surface and intermediate (LIW/CIW) waters which were the subject of sometimes divergent theories, 2 to 3 decades ago. This study verifies many results or previous theories, but it proposes on the one hand a more detailed view (spatially and seasonally) and also, in some areas, new patterns. It should also be kept in mind that our simulation is also related to a period characterized by cyclonic circulation in the Ionian Sea. Fig. 16 presents the synthesis of the results, the main elements of which are summarized here:

At the surface, the general circulation is cyclonic, alongslope, stronger and more stable in winter. In summer the current veins are sometimes interrupted as in the South Ionian where the continuity of the circulation is done by a train of eddies, or, in other cases, the current is very narrow and stuck to the coast as along the North Ionian east coast or the Middle East coast. Another notable difference between winter and summer is located to the extreme east of the basin: in winter, our surface circulation pattern is similar to that of Millot and Taupier-Letage (2005) with the exit from the Levantine through the Aegean, while in summer, the surface water exits westward south of Crete. The Aegean then tends to be isolated from the Levantine and the Ionian by large eddies, one cyclonic on the Aegean side which closes the Cretan Arc to the east and the other anticyclonic on the Ionian side which closes the Cretan Arc to the west. Pelops, Ierapetra, the Cyprus eddy and the Mersa-Matruh Eddies are anticyclonic eddies (or accumulation of eddies) recurring in both seasons. The juxtaposition of Ierapetra, Rhodes Gyre and Mersa-Matruh produces a southward path across the Levantine basin at about 27 − 28°E which delimits a large cyclonic circulation to the east which tends to separate the two parts of the basin (west and east Levantine) and thus increases the residence time in the east resulting in a pronounced zonal gradient of salinity between the two sides of this current, especially in summer at the surface.

Intermediate waters also present a seasonality that, to our knowledge, is not mentioned in the literature: while there is an alongslope cyclonic circulation all around the Levantine basin in winter, this is no longer the case in summer with an inversion of the current on the Middle East coast and no significant current in front of the Nile Delta and the Sinai. The rim current of the Rhodes Gyre and the southward path at 27-28°E ensure the dispersion of the Levantine Intermediate waters throughout the eastern Levantine in winter, while in summer, it is mainly the large anticyclonic circulation that occupies the southeast of the basin that redistributes towards the south the Levantine water.

The two paths mentioned above of surface and intermediate waters, either along southern Crete in summer or through the Aegean in winter, end in the Ionian where Pelops and the nearby high pressure areas in

both seasons seem to play a major role in the turbulent dispersion of the intermediate water north, south, and even west of the Ionian towards the Sicily Channel. The presence of recurrent anticyclones between 35 and 37°N along a band extending from west to east of the Ionian also produces a vertical dispersion of intermediate water. All these processes produce in the Ionian a significant dilution of the salt of this water mass. In the Adriatic and along the Ionian west coast, the circulation is classically cyclonic. Finally, the circulation of intermediate water in the South Ionian presents an important seasonality. In the summer a large area is affected by an anticyclonic circulation that seems to be wind induced and around which wraps intermediate water that has not transited through the northern Ionian and arrives a little more salty to the Sicily Channel.

All the sub-basins of the Eastern Mediterranean are characterized by mesoscale circulations that give a strong imprint, both on the pathways steered by vortex assemblages that create "pseudo current veins" or by a multidirectional dispersion as in the North Ionian. We believe that the representation of these structures is fundamental to correctly represent the residence times of water masses in the Eastern Mediterranean and the transformations undergone by its constituents. Intermediate Water is the pathway of organic matter that falls from the upper part of the water column and reaches the western Mediterranean after recycling and consumption of oxygen. Modelling these transformations requires a correct representation of transit times and mixing with the surrounding water.

The results of this paper are presented in climatological mode (average over 8 years). In a future paper, this simulation will be used in addition to the previous Argo-based studies (Kassis and Korres, 2020 ; Kokkini et al., 2020) to quantify the interannual variability of water formations in the different sub-basins as well as the trends in the characteristics of water masses over the last decade. The very good reproduction by the model of the Argo time series pleads for a realistic representation of these trends.

6. Data availability

The distribution of the simulations is provided by the national SI-ROCCO service, funded by CNRS-INSU and the University of Toulouse and supported by the ILICO research infrastructure. Simulations are available in netcdf format upon request to the authors.

Declaration of Competing Interest

The authors declare that they have no known competing financial interests or personal relationships that could have appeared to influence the work reported in this paper.

Acknowledgements

The authors warmly acknowledge the international ARGO program for supporting the deployment of profilers. Argo data were collected and made freely available by the CORIOLIS project (http://www.coriolis.eu.org) and programs that contribute to it. The outputs of the operational oceanic model used for the boundary conditions were provided by Mercator-Ocean International. The atmospheric fields were provided by ECMWF. We thank Françoise Orain from Météo-France for her help with the SST images. Rivers discharge were downloaded from Settore Idrologico e Geologico Regionale from Toscane Region for Arno, ARPAE (Agenzio Prevenzione Ambiante Energia Emilia Romagna) for Po, SAIH-Ebro for Ebro, Banque Hydro for French rivers. Numerical simulations were performed using HPC resources from CALMIP (grants P09115 and P1325) and from GENCI and CINES (Grand Equipement National de Calcul Intensif, project A0040110088). This study is a contribution to the MerMex (Marine Ecosystem Response in the Mediterranean Experiment) and HyMeX (Hydrological cycle in the Mediterranean EXperiment) projects of the MISTRALS international program.

Appendix A:. The VQS coordinate

The VQS coordinate uses the sigma coordinate with an "envelope bathymetry" instead of the true bathymetry. The "envelope bathymetry" is always below and smoother than the true bathymetry. In Siddorn and Furner (2013), the grid points below the seafloor are masked. In our case, these points are not masked but stuck under the bottom. During the simulation, these ghost points will receive the value of the first level above the bottom, thus reinforcing the horizontal continuity of the advective and diffusive fluxes requiring the value of these particular points. In our case, the implementation of the VQS coordinate highlighted three issues: (1) the numerical stability of the advection, (2) the accuracy of the pressure gradient force (PGF), (3) the continuity of the bottom flow.

Numerical stability of the advection

The problem of numerical instability of the advection arises for large values of the current number ($c_n = u\Delta t/\Delta x$). We use the QUICKEST tracer advection scheme. For regular grid cells, the maximum theoretical value allowed for c_n is 1. In this particular case, the QUICKEST scheme becomes equivalent to a basic upwind scheme (Leonard, 1979, see A.7 for $c_n = 1$), the horizontal fluxes of the tracers being simply $u_{i+1/2}T_i$ and $u_{i-1/2}T_{i-1}$ when $u > 0$. The discrete form of the divergence of horizontal fluxes, derived from the sigma coordinate (including the spatial variation in cell thickness), then approaches$\Delta z_i^{t+1}T_i^{t+1} = \Delta z_i^t T_i^t + \Delta t/\Delta x\left(\Delta z_{i-1/2}^t u_{i-1/2}T_{i-1} - \Delta z_{i+1/2}^t u_{i+1/2}T_i\right)$, equivalent (if we neglect the temporal variations of the cell thickness) to $T_i^{t+1} = \left(1 - \frac{\Delta z_{i+1/2}}{\Delta z_i}\frac{\Delta t u_{i+1/2}}{\Delta x}\right)T_i^t + \frac{\Delta z_{i-1/2}}{\Delta z_i}\frac{\Delta t u_{i-1/2}}{\Delta x}T_{i-1}^t$, where the factor coefficients of T_i^t and T_{i-1}^t must be between 0 and 1 for the scheme to be stable. However, this criterion is easily not met in the first layer above the bottom by all tracer cells whose thickness is significantly smaller than those of the neighbouring current cells, i.e.$\Delta z_{i+1/2}/\Delta z_i \gg 1$ or $\Delta z_{i-1/2}/\Delta z_i \gg 1$ (Fig. A1). To counter this problem, the first two layers above the bottom are merged into a single layer, with velocities and tracers being weighted averaged before being combined to calculate the fluxes. The advection scheme then shifts the average tracer value. Once the advection step is complete, a realistic vertical profile is reconstructed over these two layers (without changing the mean) so as not to affect the accuracy of the PGF and buoyancy term in the turbulent kinetic energy equation (which would otherwise be zero). This vertical profile is deduced by continuity with the upper layers.

Accuracy of the pressure gradient force (PGF)

We use the Jacobian Pressure scheme detailed in Marsaleix et al. (2009, 2011). The first layer above the bottom can degrade the accuracy of the PGF due to the asymmetry of the cell shape, caused by the slope of its lower facet (which coincides with that of the bottom), potentially much steeper than that of the upper facet (Fig. A1). Without changing the formulation of the scheme, the PGF is thus calculated on a sub-cell within the first cell of the bottom. This sub-cell restores symmetry properties, with two vertical sides of comparable thicknesses and a new lower facet, almost parallel to the (unchanged) upper facet. The lower facet is entirely above the bottom to avoid the inaccuracy of extrapolating the fields below the bathymetry.

Continuity of the bottom flow

The abrupt change in cell thickness, each time the VQS coordinate jumps a step, can degrade the horizontal continuity of the velocity field near the bottom. The main cause is bottom friction, despite the fact that the logarithmic layer is theoretically insensitive to vertical resolution. However, this property is not verified if the vertical resolution is insufficient. The problem is further exacerbated by the fact that the formulation of the bottom friction is highly non-linear, by the quadratic dependence on the current and because the formulation of the drag coefficient is dependent on the height above the bottom of the current under consideration. To counteract this problem a "continuous" virtual bottom layer is constructed (Fig. A2). Its thickness is given by the thickness Δz_{kb+1} of the second layer above the bottom. The bottom friction is calculated at the centre of this virtual cell, i.e. at a distance from the bottom equal to $0.5\Delta z_{kb+1}$, using a drag coefficient given by $c_D = (0.40/ln(0.5\Delta z_{kb+1}/z_0))^2$ where z_0 is a roughness length. Then, a virtual bottom velocity is reconstructed from a weighted average of the velocities of the first two levels above the bottom. This weighted average depends on the overlap of the virtual layer with the two layers above the bottom, in practice:$u_b = \Delta z_{kb}/\Delta z_{kb+1} u_{kb} + (\Delta z_{kb+1} - \Delta z_{kb})/\Delta z_{kb+1} u_{kb+1}$ where kb and $kb+1$ are the first and second level above the bottom respectively. The equation for $u\Delta z$ considers a bottom friction that is split between the levels kb and $kb+1$, i.e. respectively $c_D\left(u_b^2+v_b^2\right)^{1/2}(\Delta z_{kb}/\Delta z_{kb+1})u_{kb}^{t+1}$ and $c_D\left(u_b^2+v_b^2\right)^{1/2}((\Delta z_{kb+1}-\Delta z_{kb})/\Delta z_{kb+1})u_{kb+1}^{t+1}$, the sum of which verifies $c_D\left(u_b^2+v_b^2\right)^{1/2}u_b^{t+1}$ and where the time indices $t+1$ indicate that the calculation is processed implicitly.

Appendix B:. Evaluation of temperature with Argo

See Fig. B1

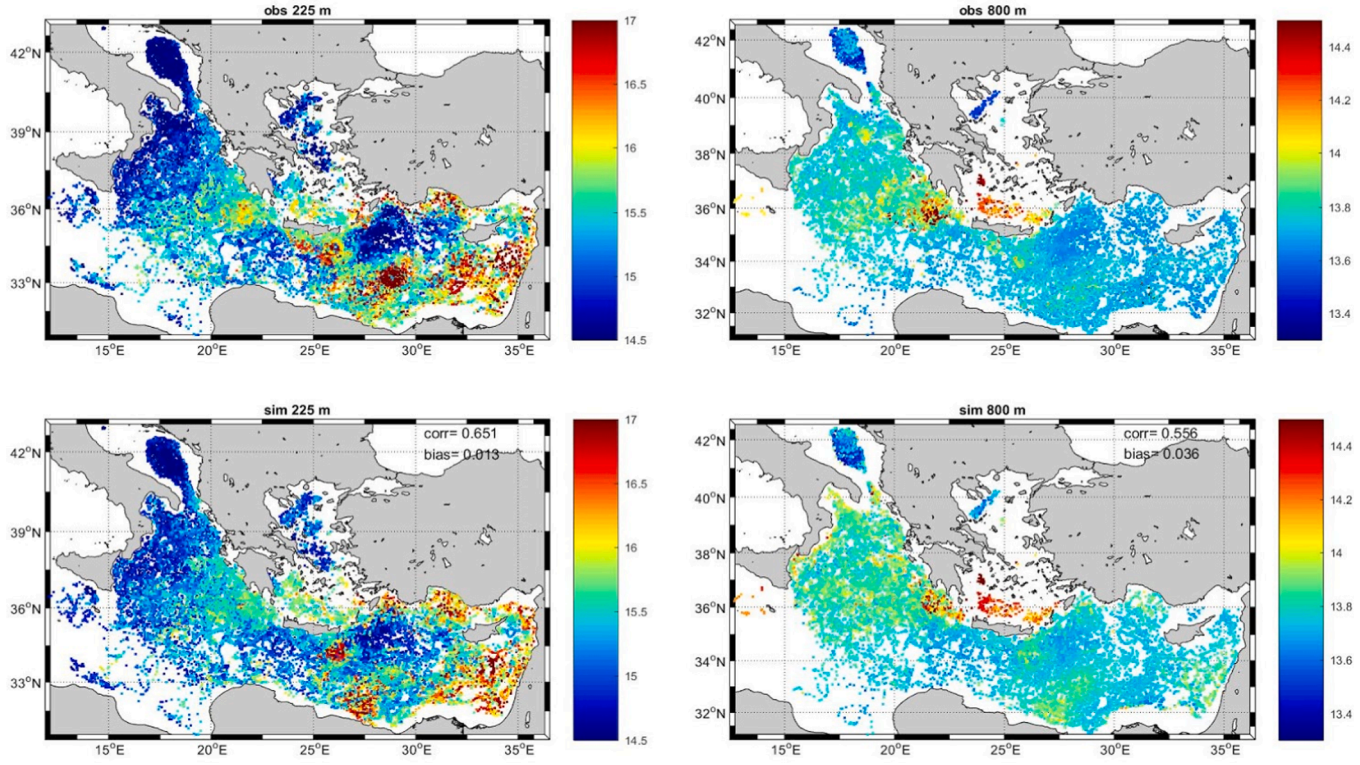

Fig. B1. Temperature observed (top) and simulated (bottom) at 225 m (left) and 800 m (right) as shown in the figure. Each point corresponds to an observed / simulated Argo profile. The temperature range common to the observed and simulated values is adapted to each depth.

References

Alhammoud, B., Béranger, K., Mortier, L., Crépon, M., Dekeyser, I., 2005. Surface circulation of the Levantine Basin: Comparison of model results with observations. Progress in Oceanography 66, 299–320.

Arnone, R.A., La Violette, P.E., 1986. Satellite Definition of the Bio-Optical and Thermal Variation of coastal eddies associated with the African Current. J. Geophys. Res. 91 (C2), 2351–2364.

Astraldi, M., Balopoulos, S., Candela, J., Font, J., Gacic, M., Gasparini, G.P., Manca, B., Theocharis, A., Tintore, J., 1999. The role of straits and channels in understanding the characteristics of Mediterranean circulation. Progress in Oceanography 44 (1–3), 65–108.

Bensi, M., Velaoras, D., Meccia, V.L., Cardin, V., 2016. Effects of the Eastern Mediterranean Sea circulation on the thermohaline properties as recorded by fixed deep-ocean observatories. Deep-Sea Research I 112, 1–13.

Béranger, K., Mortier, L., Gasparini, G.-P., Gervasio, L., Astraldi, M., Crépon, M., 2004. The dynamics of the Sicily Strait: a comprehensive study from observations and models. Deep-Sea Research II 51, 411–440.

Béranger, K., Mortier, L., Crépon, M., 2005. Seasonal variability of water transport through the Straits of Gibraltar, Sicily and Corsica, derived from a high-resolution model of the Mediterranean circulation. Progress in Oceanography 66, 341–364.

Béthoux, J.P., 1980. Mean water fluxes across sections in the Mediterranean Sea, evaluated on the basis of water and salt budgets and of observed salinities. Oceanologica Acta 3, 79–88.

Beuvier, J., Sevault, F., Herrmann, M., Kontoyiannis, H., Ludwig, W., Rixen, M., Stanev, E., Béranger, K., Somot, S., 2010. Modeling the Mediterranean Sea interannual variability during 1961–2000: Focus on the Eastern MediterraneanTransient. J. Geophys. Res. 115, C08017. https://doi.org/10.1029/2009JC005950.

Beuvier, J., Béranger, K., Brossier, C.L., Somot, S., Sevault, F., Drillet, Y., Bourdallé, B.R., Ferry, N., Lyard, F., 2012. Spreading of the western Mediterranean deep water after winter 2005: Time scales and deep cyclone transport. J. Geophys. Res. 117, C07022. https://doi.org/10.1029/2011JC007679.

Civitarese, G., Gačić, M., Lipizer, M., Eusebi Borzelli, G.L., 2010. On the impact of the Bimodal Oscillating System (BiOS) on the biogeochemistry and biology of the Adriatic and Ionian Seas (Eastern Mediterranean). Biogeosciences 7, 3987–3997. https://doi.org/10.5194/bg-7-3987-2010.

Damien, P., Bosse, A., Testor, P., Marsaleix, P., Estournel, C., 2017. Modeling postconvective submesoscale coherent vortices in the northwestern Mediterranean Sea. J. Geophys. Res. Oceans 122. https://doi.org/10.1002/2016JC012114.

Dukhovskoy, D.S., Morey, S.L., Martin, P.J., O'Brien, J.J., Cooper, C., 2009. Application of a vanishing, quasi-sigma, vertical coordinate for simulation of high-speed, deep currents over the Sigsbee Escarpment in the Gulf of Mexico. Ocean Modelling 28, 250–265.

Estournel, C., Durrieu de Madron, X., Marsaleix, P., Auclair, F., Julliand, C., Vehil, R., 2003. Observation and modelisation of the winter coastal oceanic circulation in the Gulf of Lions under wind conditions influenced by the continental orography (FETCH experiment). Journal of Geophysical Res. 108 (C3), 8059. https://doi.org/10.1029/2001JC000825.

Estournel, C., Zervakis, V., Marsaleix, P., Papadopoulos, A., Auclair, F., Perivoliotis, L., Tragou, E., 2005. Dense water formation and cascading in the Gulf of Thermaikos (North Aegean) from observations and modelling. Continental Shelf Research 25, 2366–2386.

Estournel, C., Testor, P., Damien, P., D'Ortenzio, F., Marsaleix, P., Conan, P., Kessouri, F., Durrieu de Madron, X., Coppola, L., Lellouche, J.-M., Belamari, S., Mortier, L., Ulses, C., Bouin, M.-N., Prieur, L., 2016. High resolution modeling of dense water formation in the north-western Mediterranean during winter 2012–2013: Processes and budget. J. Geophys. Res. Oceans 121, 5367–5392. https://doi.org/10.1002/2016JC011935.

Fach, B.A., Orek, H., Yilmaz, E., Tezcan, D., Salihoglu, I., Salihoglu, B., Latif, M.A., 2021. Water mass variability and Levantine Intermediate Water formation in the Eastern Mediterranean between 2015 and 2017. e2020JC016472 Journal of Geophysical Research: Oceans 126. https://doi.org/10.1029/2020JC016472.

Fairall, C.W., Bradley, E.F., Hare, J.E., Grachev, A.A., Edson, J.B., 2003. Bulk Parameterization of Air-Sea Fluxes: Updates and Verification for the COARE Algorithm. Journal of Climate 16 (4), 571–591. https://doi.org/10.1175/1520-0442(2003)016<0571:BPOASF>2.0.CO;2.

Gačić, M., Eusebi Borzelli, G.L., Civitarese, G., Cardin, V., Yari, S., 2010. Can internal processes sustain reversals of ocean upper circulation? The Ionian Sea example. Geophys. Res. Lett. 37, L09608. https://doi.org/10.1029/2010GL043216.

Gačić, M., Civitarese, G., Eusebi Borzelli, G.L., Kovačević, V., Poulain, P.-M., Theocharis, A., Menna, M., Catucci, A., Zarokanellos, N., 2011. On the relationship between the decadal oscillations of the northern Ionian Sea and the salinity distributions in the eastern Mediterranean. J. Geophys. Res. 116, C12002. https://doi.org/10.1029/2011JC007280.

Gačić M., Civitarese G., Kovačević V., Ursella L., Bensi M., Menna M., Cardin V., Poulain P.-M. , Cosoli S., Notarstefano G. and C. Pizzi, 2014. Extreme winter 2012 in the Adriatic: an example of climatic effect on the BiOS rhythm. Ocean Sci., 10, 513–522.

García, M.J.L., Millot, C., Font, J., García-Ladona, E., 1994. Surface circulation variability in the Balearic Basin. J. Geophys. Res. 99 (C2), 3285–3296. https://doi.org/10.1029/93JC02114.

Gerin, R., Poulain, P.-M., Taupier-Letage, I., Millot, C., Ben, Ismail S., Sammari, C., 2009. Ocean Sci. 5, 559–574.

Gerin, R., Kourafalou, V., Poulain, P.-M., Besiktepe, Ş., 2014. Influence of Dardanelles outflow induced thermal fronts and winds on drifter trajectories in the Aegean Sea. Mediterranean Marine Science 15 (2), 239–249. https://doi.org/10.12681/mms.464.

Georgopoulos, D., Theocharis, A., Zodiatis, G., 1989. Intermediate water formation in the Cretan Sea (South Aegean Sea). Oceanologica Acta 12 (4), 353–359.

Graham J. A., O'Dea E., Holt J., Polton J., Hewitt H. T., Furner R., Guihou K., Brereton A., Arnold A., Wakelin S., Castillo Sanchez J. M. and C.G. Mayorga Adame, 2018. AMM15: a new high-resolution NEMO configuration for operational simulation of the European north-west shelf. Geoscientific Model Development, 11, 681-696, doi: 10.5194/gmd-11-681-2018.

Hamad, N., Millot, C., Taupier-Letage, I., 2005. A new hypothesis about the surface circulation in the eastern basin of the Mediterranean Sea. Prog. Oceanogr. 66, 287–298. https://doi.org/10.1016/j.pocean.2005.04.002.

Hamad, N., Millot, C., Taupier-Letage, I., 2006. The Surface Circulation in the Eastern Basin of the Mediterranean Sea. Scientia Marina 70, 457–503.

Hayes, D.R., Schroeder, K., Poulain, P.-M., Testor, P., Mortier, L., Bosse, A., Durrieu de Madron, X., 2019. Review of the Circulation and Characteristics of Intermediate Water Masses of the Mediterranean: Implications for Cold-Water Coral Habitats. In: Orejas, C., Jiménez, C. (Eds.), Mediterranean Cold-Water Corals: Past, Present and Future. Coral Reefs of the World, vol 9. Springer, Cham. https://doi.org/10.1007/978-3-319-91608-8_18.

Herbaut, C., Martel, F., Crépon, M., 1997. A Sensitivity Study of the General Circulation of the Western Mediterranean Sea. Part II: The Response to Atmospheric Forcing. Journal of Physical Oceanography 27, 2126–2145.

Herrmann, M., Estournel, C., Déqué, M., Marsaleix, P., Sevault, F., Somot, S., 2008. Dense water formation in the Gulf of Lions shelf: Impact of atmospheric interannual variability and climate change. Continental Shelf Research 28 (15), 2092–2112.

Ioannou, A., Stegner, A., Le Vu, B., Taupier-Letage, I., Speich, S., 2017. Dynamical evolution of intense Ierapetra eddies on a 22 year long period. Journal of Geophysical Research: Oceans 122. https://doi.org/10.1002/2017JC013158.

Ioannou, A., Stegner, A., Tuel, A., LeVu, B., Dumas, F., Speich, S., 2019. Cyclostrophic corrections of AVISO/DUACS surface velocities and its application to mesoscale eddies in the Mediterranean Sea. Journal of Geophysical Research: Oceans 124, 8913–8932. https://doi.org/10.1029/2019JC015031.

Janeković I., Mihanović H., Vilibić I. and M. Tudor, 2014. Extreme cooling and dense water formation estimates in open and coastal regions of the Adriatic Sea during the winter of 2012. J. Geophys. Res. Oceans, 119, 3200–3218, doi:10.1002/2014JC009865.

Jebri, F., Birol, F., Zakardjian, B., Bouffard, J., Sammari, C., 2016. Exploiting coastal altimetry to improve the surface circulation scheme over the central Mediterranean Sea. J. Geophys. Res. Oceans 121, 4888–4909. https://doi.org/10.1002/2016JC011961.

Kassis, D., Korres, G., 2020. Hydrography of the Eastern Mediterranean basin derived from argo floats profile data. Deep-Sea Research II 171, 104712.

Katz T., Weinstein Y., Alkalay R., Biton E., Toledo Y., Lazar A., Zlatkin O., Soffer R., Rahav E., Sisma-Ventura G., Bar T., Ozer T., Gildor H., Almogi-Labin A., Kanari M., Berman-Frank I. and B.Herut, 2020. The first deep-sea mooring station in the eastern Levantine basin (DeepLev), outline and insights into regional sedimentological processes, Deep Sea Research Part II: Topical Studies in Oceanography,Volume 171,104663,doi:10.1016/j.dsr2.2019.104663.

Kessouri, F., Ulses, C., Estournel, C., Marsaleix, P., D'Ortenzio, F., Severin, T., et al., 2018. Vertical mixing effects on phytoplankton dynamics and organic carbon export in the western Mediterranean Sea. Journal of Geophysical Research: Oceans 123, 1647–1669. https://doi.org/10.1002/2016JC012669.

Kokkini, Z., Mauri, E., Gerin, R., Poulain, P.M., Simoncelli, S., Notarstefano, G., 2020. On the salinity structure in the South Adriatic as derived from float and glider observations in 2013–2016. Deep-Sea Research Part II 171, 104625.

Kontoyiannis, H., Theocharis, A., Balopoulos, E., Kioroglou, S., Papadopoulos, V., Collins, M., Velegrakis, A.F., Iona, A., 1999. Water fluxes through the Cretan Arc Straits, Eastern Mediterranean Sea: March 1994 to June 1995. Progress in Oceanography 44, 511–529.

Kontoyiannis, H., Kourafalou, V.H., Papadopoulos, V., 2003. Seasonal characteristics of the hydrology and circulation in the northwest Aegean Sea (eastern Mediterranean): Observations and modeling. J. Geophys. Res. 108 (3302), C9. https://doi.org/10.1029/2001JC001132.

Krajcar, V., 2003. Climatology of geostrophic currents in the Northern Adriatic. Geofizika 20.

Krokos, K., Velaoras, D., Korres, G., Perivoliotis, L., Theocharis, A., 2014. On the continuous functioning of an internal mechanism that drives the Eastern Mediterranean thermohaline circulation: The recent activation of the Aegean Sea as a dense water source area. Journal of Marine Systems 129, 484–489.

Kubin, E., Poulain, P.-M., Mauri, E., Menna, M., Notarstefano, G., 2019. Levantine Intermediate and Levantine Deep Water Formation: An Argo Float Study from 2001 to 2017. Water 11, 1781. https://doi.org/10.3390/w11091781.

Lacombe, H., Tchernia, P., 1960. Quelques traits généraux de l'hydrologie méditerranéenne. Cah. Océanogr. 12, 527–547.

Lacombe H. and P. Tchernia, 1972. Caractères hydrologiques et circulation des eaux en Méditerranée, in : The Mediterranean Sea: A Natural Sedimentation Laboratory, edited by D. J. Stanley, Dowden, Hutchinson and Ross, Stroudsburg, PA, 25-36.

Lascaratos, A., Williams, R.G., Tragou, E., 1993. A Mixed-Layer Study of the Formation of Levantine Intermediate Water. J. Geophys. Res. 98 (C8), 739–749.

Lascaratos, A., Nittis, K., 1998. A high-resolution three-dimensional numerical study of intermediate water formation in the Levantine Sea. J. Geophys. Res. 103 (C9), 18497–18511.

Lellouche, J.-M., et al., 2013. Evaluation of global monitoring and forecasting systems at Mercator Ocean. Ocean Sci. 9, 57–81. https://doi.org/10.5194/os-9-57-2013.

Leonard, B.P., 1979. A stable and accurate convective modelling procedure based on quadratic upstream interpolation. Comput. Methods Appl. Mech. Eng. 19, 59–98.
Ludwig, W., Dumont, E., Meybeck, M., Heussner, S., 2009. River discharges of water and nutrients to the Mediterranean and Black Sea: Major drivers for ecosystem changes during past and future decades? Progress in Oceanography 80, 199–217.
Lyard, F.H., Allain, D.J., Cancet, M., Carrère, L., Picot, N., 2020. FES2014 global ocean tides atlas: design and performances. Ocean Sci. Discuss. https://doi.org/10.5194/os-2020-96.
Macias, D., Cózar, A., Garcia-Gorriz, E., González-Fernández, D., Stips, A., 2019. Surface water circulation develops seasonally changing patterns of floating litter accumulation in the Mediterranean Sea. A modelling approach. Marine Pollution Bulletin 149, 110619. https://doi.org/10.1016/j.marpolbul.2019.110619.
Malanotte-Rizzoli, P., Hecht, A., 1988. Large-scale properties of the Eastern Mediterranean: a review. Oceanologica Acta 11, 4.
Malanotte-Rizzoli, P., Robinson, A.R., 1988. POEM: physical oceanography of the eastern Mediterranean. Eos 69, 14.
Malanotte-Rizzoli, P., Manca, B.B., Ribera, d'Alcala M., Theocharis, A., et al., 1997. A synthesis of the Ionian Sea hydrography, circulation and water mass pathways during POEM-Phase I. Prog. Oceanogr. 39, 153–204.
Malanotte-Rizzoli, P., Manca, B.B., Ribera, d'Alcala M., Theocharis, A., Brenner, S., Budillon, G., Ozsoy, E., 1999. The Eastern Mediterranean in the 80s and in the 90s: the big transition in the intermediate and deep circulations. Dynamics of Atmospheres and Oceans 29, 365–395.
Manca, B., Kovačević, V., Gačić, M., Viezzoli, D., 2002. Dense water formation in the Southern Adriatic Sea and spreading into the Ionian Sea in the period 1997–1999. J. Mar. Syst. 33–34, 133–154.
Mantziafou, A., Lascaratos, A., 2004. An eddy resolving numerical study of the general circulation and deep-water formation in the Adriatic Sea. Deep Sea Research Part I 51 (7), 921–952.
Manzella, G.M.R., Gasparini, G.P., Astraldi, M., 1988. Water exchange between the eastern and western Mediterranean through the Strait of Sicily. Deep-Sea Research 35 (6), 1021–1035.
Marsaleix, P., Auclair, F., Floor, J.W., Herrmann, M.J., Estournel, C., Pairaud, I., Ulses, C., 2008. Energy conservation issues in sigma-coordinate free-surface ocean models. Ocean Modelling. 20, 61–89.
Marsaleix P., Auclair F. and C. Estournel C. and I. Pairaud, 2006. Considerations on open boundary conditions for regional and coastal ocean models. J. Atmos. and Oceanic Technol., 23,1604-1613.
Marsaleix, P., Auclair, F., Estournel, C., Nguyen, C., Ulses, C., 2011. An accurate implementation of the compressibility terms in the equation of state in a low order pressure gradient scheme for sigma coordinate ocean models. Ocean Modelling 40, 1–13.
Marsaleix, P., Auclair, F., Estournel, C., 2009. Low-order pressure gradient schemes in sigma coordinate models: The seamount test revisited. Ocean Modelling 30, 169–177.
MEDOC Group, 1970. Observation of formation of deep water in the Mediterranean Sea, 1969. Nature, Vol. 227, September 5 1970.
Menna, M., Poulain, P.-M., 2010. Mediterranean intermediate circulation estimated from Argo data in 2003–2010. Ocean Sci. 6, 331–343.
Menna, M., Poulain, P.-M., Zodiatis, G., Gertman, I., 2012. On the surface circulation of the Levantine sub-basin derived from Lagrangian drifters and satellite altimetry data. Deep-Sea Research I 65, 46–58.
Menna, M., Reyes Suarez, N.C., Civitarese, G., Gačić, M., Rubino, A., Poulain, P.-M., 2019a. Decadal variations of circulation in the Central Mediterranean and its interactions with mesoscale gyres. Deep-Sea Research Part II 164, 14–24.
Menna, M., Poulain, P.-M., Ciani, D., Doglioli, A., Notarstefano, G., Gerin, R., Rio, M.-H., Santoleri, R., Gauci, A., Drago, A., 2019b. New Insights of the Sicily Channel and Southern Tyrrhenian Sea Variability. Water 2019 (11), 1355. https://doi.org/10.3390/w11071355.
Menna, M., Notarstefano, G., Poulain, P.-M., Mauri, E., Falco, P. and E. Zambianchi, 2020. Surface picture of the Levantine Basin as derived by drifter and satellite data, Section 3.5 of von Schuckmann et al., 2020, Copernicus Marine Service Ocean State Report, 4, Journal of Operational Oceanography, S1-S172, DOI: 10.1080/1755876X.2020.1785097.
Millot, C., 1987. Circulation in the western Mediterranean Sea. Oceanol. Acta 10 (2), 143–149.
Millot, C., Taupier-Letage, I., 2005. Circulation in the Mediterranean Sea. In: Saliot, A. (Ed.), The Handbook of Environmental Chemistry 5 (K). Springer-Verlag, Heidelberg, pp. 29–66.
Mkhinini, N., Santi Coimbra, A.L., Stegner, A., Arsouze, T., Taupier-Letage, I., Beranger, K., 2014. Long-lived mesoscale eddies in the eastern Mediterranean Sea: Analysis of 20 years of AVISO geostrophic velocities. J. Geophys. Res. Oceans 119, 8603–8626. https://doi.org/10.1002/2014JC010176.
Nielsen, J.N., 1912. Hydrography of the Mediterranean and adjacent waters. Rep. Dan. Oceanogr. Exped. 1908–1910, 77–192.
Nittis, K., Perivoliotis, L., 2002. Circulation and hydrological characteristics of the North Aegean Sea: a contribution from real-time buoy measurements. Mediterranean Marine Science 3 (1), 21–32. https://doi.org/10.12681/mms.255.
Nixon, S.W., 2003. Replacing the Nile: Are anthropogenic nutrients providing the fertility once brought to the Mediterranean by a great river? Ambio 32, 30–39.
Notarstefano, G., Menna, M., Legeais, J.F., 2019. Reversal of the Northern Ionian circulation in 2017, Section 4.5 of von Schuckmann et al., 2019, Copernicus Marine Service Ocean State Report, 3.Journal of Operational. Oceanography 12, S108. https://doi.org/10.1080/1755876X.2019.1633075.
Ovchinnikov, M., 1966. Circulation in the surface and intermediate layers of the Mediterranean Sea. Oceanology 6, 48–59.
Ozer, T., Gertman, I., Kress, N., Silverman, J., Herut, B., 2017. Interannual thermohaline (1979–2014) and nutrient (2002–2014) dynamics in the Levantine surface and intermediate water masses. SE Mediterranean Sea, Global and Planetary Change 151, 60–67. https://doi.org/10.1016/j.gloplacha.2016.04.001.
Özsoy, E., Hecht, A., Unluata, U., 1989. Circulation and hydrography in the Levantine basin: results of POEM coordinated experiments 1985–1986. Prog. Oceanogr. 22, 125–170.
Özsoy, E., Unluata, U., Oguz, T., Latif, M.A., Hecht, A., Brenner, S., Bishop, J., Rozentraub, Z., 1991. A review of the Levantine Basin Circulation and its variabilities during 1985–1988. Dyn. Atmos. Oceans 15, 421–456.
Özsoy, E., Hecht, A., Ünlüata, Ü., Brenner, S., Sur, H.I., Bishop, J., Latif, M.A., Rozentraub, Z., Oguz, T., 1993. A synthesis of the Levantine Basin circulation and hydrography, 1985–1990. Deep-Sea Res. 40, 1075–1119.
Pairaud, I.L., Lyard, F., Auclair, F., Letellier, T., Marsaleix, P., 2008. Dynamics of the semi-diurnal and quarter-diurnal internal tides in the Bay of Biscay. Part 1: Barotropic tides. Continental Shelf Research 28, 1294–1315. https://doi.org/10.1016/j.csr.2008.03.004.
Pascual, A., Buongiorno, Nardelli B., Larnicol, G., Emelianov, M., Gomis, D., 2002. A case of an intense anticyclonic eddy in the Balearic Sea (western Mediterranean). J. Geophys. Res. 107 (C11), 3183. https://doi.org/10.1029/2001JC000913.
Pascual, A., Pujol, M.-I., Larnicol, G., Le Traon, P.-Y., Rio, M.-H., 2007. Mesoscale mapping capabilities of multisatellite altimeter missions: First results with real data in the Mediterranean Sea. Journal of Marine Systems 65, 190–211.
Paulson, C.A., Simpson, J.J., 1977. Irradiance measurements in the upper ocean. J. Phys. Oceanogr. 7, 952–956.
Pinardi, N., Navarra, A., 1993. Baroclinic wind adjustment processes in the Mediterranean sea. Deep Sea Research II 40 (6), 1299–1326.
Pinardi, N., Zavatarelli, M., Adani, M., Coppini, G., Fratianni, C., Oddo, P., Simoncelli, S., Tonani, M., Lyubartsev, V., Dobricic, S., Bonaduce, A., 2015. Mediterranean Sea large-scale low-frequency ocean variability and water mass formation rates from 1987 to 2007: A retrospective analysis. Progress in Oceanography 132, 318–332. https://doi.org/10.1016/j.pocean.2013.11.003.
Poulain, P.-M., 2001. Adriatic Sea surface circulation as derived from drifter data between 1990 and 1999. Journal of Marine Systems 29, 3–32.
Poulos, S.E., Drakopoulos, P.G., Collins, M.B., 1997. Seasonal variability in sea surface oceanographic conditions in the Aegean Sea (Eastern Mediterranean): an overview. Journal of Marine Systems 13, 225–244.
Rio, M.-H., Poulain, P.-M., Pascual, A., Mauri, E., Larnicol, G., Santoleri, R., 2007. A Mean Dynamic Topography of the Mediterranean Sea computed from altimetric data, in-situ measurements and a general circulation model. Journal of Marine Systems 65, 484–508.
Robinson, A.R., Golnaraghi, M., Leslie, N., Artegiani, A., Hecht, A., Lazzone, E., Michelato, A., Sanzone, E., Theocharis, A., Unluata, U., 1991. Structure and variability of the Eastern Mediterranean general circulation. Dyn. Atmos. Oceans 15, 215–240.
Robinson, A.R., Golnaraghi, M., 1993. Circulation and dynamics of the Eastern Mediterranean Sea; quasi-synoptic data-driven simulations. Deep Sea Res. 40 (6), 1207–1246.
Sammari, C., Millot, C., Prieur, L., 1995. Aspects of the seasonal and mesoscale variabilities of the Northern Current in the western Mediterranean Sea inferred from the PROLIG-2 and PROS-6 experiments. Deep Sea Research Part I: Oceanographic Research Papers Vol. 42, Issue 6.
Sannino G., Sánchez Garrido J.C., Liberti L. and L. Pratt, 2014. Exchange flow through the Strait of Gibraltar as simulated by a σ-coordinate hydrostatic model and a z-coordinate nonhydrostatic model. In G.L. Eusebi Borzelli, M. Gačić, P. Lionello, P. Malanotte-Rizzoli (eds), The Mediterranean Sea: Temporal Variability and Spatial Patterns. doi:10.1002/9781118847572, Geophysical Monograph Series.
Schlitzer, R., Roether, W., Oster, H., Junghans, H.-G., Hausmann, M., Johannsen, H., Michelato, A., 1991. Chlorofluoromethane and oxygen in the Eastern Mediterranean. Deep-Sea Research. Vol. 38, 12, 1531–1551.
Seyfried, L., Marsaleix, P., Richard, E., Estournel, C., 2017. Modelling deep-water formation in the North-West Mediterranean Sea with a new air-sea coupled model: sensitivity to turbulent flux parameterizations. Ocean Sci. 13, 1093–1112. https://doi.org/10.5194/os-13-1093-2017.
Seyfried, L., Estournel, C., Marsaleix, P., Richard, E., 2019. Dynamics of the North Balearic Front during an autumn tramontane and mistral storm: air–sea coupling processes and stratification budget diagnostic. Ocean Sci. 15, 179–198. https://doi.org/10.5194/os-15-179-2019.
Siddorn, J.R., Furner, R., 2013. An analytical stretching function that combines the best attributes of geopotential and terrain-following vertical coordinates. Ocean Modelling 66, 1–13.
Somot, S., Houpert, L., Sevault, F., et al., 2016. Characterizing, modelling and understanding the climate variability of the deep water formation in the North-Western Mediterranean Sea. Clim Dyn 51, 1179–1210. https://doi.org/10.1007/s00382-016-3295-0.
Sorgente, R., Olita, A., Oddo, P., Fazioli, L., Ribotti, A., 2011. Numerical simulation and decomposition of kinetic energies in the Central Mediterranean Sea: Insight on mesoscale circulation and energy conversion, Ocean Sci. Discuss. 8, 1–54.
Soto-Navarro, J., Somot, S., Sevault, F., et al., 2015. Evaluation of regional ocean circulation models for the Mediterranean Sea at the Strait of Gibraltar: volume transport and thermohaline properties of the outflow. Clim Dyn 44, 1277–1292. https://doi.org/10.1007/s00382-014-2179-4.
Soto-Navarro, J., Jordá, G., Amores, A., Cabos, W., Somot, S., Sevault, F., Macías, D., Djurdjevic, V., Sannino, G., Li, L., Sein, D., 2020. Evolution of Mediterranean Sea water properties under climate change scenarios in the Med-CORDEX ensemble. Climate Dynamics. https://doi.org/10.1007/s00382-019-05105-4.

Testor, P., Bosse, A., Houpert, L., Margirier, F., Mortier, L., Legoff, H., Conan, P., 2018. Multiscale observations of deep convection in the northwestern Mediterranean Sea during winter 2012–2013 using multiple platforms. Journal of Geophysical Research: Oceans 123. https://doi.org/10.1002/2016JC012671.

Theocharis, A., Georgopoulos, D., Lascaratos, A., Nittis, K., 1993. Water masses and circulation in the central region of the Eastern Mediterranean (E. Ionian, S. Aegean and NW Levantine). Deep-Sea Research II 40, 1121–1142.

Theocharis, A., Balopoulos, E., Kioroglou, S., Kontoyiannis, H., Iona, A., 1999. A synthesis of the circulation and hydrography of the South Aegean Sea and the Straits of the Cretan Arc (March 1994–January 1995). Progress in Oceanography 44, 469–509.

Theocharis A., Krokos G., Velaoras D. and G. Korres, 2014. An internal mechanism driving the alternation of the Eastern Mediterranean dense/deep water sources. in: The Mediterranean Sea: Temporal Variability and Spatial Patterns, Geophysical Monograph 202. Edited by Borzelli, Gacic, Lionello, and Malanotte-Rizzoli. American Geophysical Union.

Tugrul, S., Besiktepe, T., Salihoglu, I., 2002. Nutrient exchange fluxes between the Aegean and Black Seas through the Marmara Sea. Mediterranean Marine Science 3 (1), 33–42. https://doi.org/10.12681/mms.256.

Ulses, C., Estournel, C., Fourrier, M., Coppola, L., Kessouri, F., Lefèvre, D., Marsaleix, P., 2021. Oxygen budget of the north-western Mediterranean deep- convection region. Biogeosciences 18, 937–960. https://doi.org/10.5194/bg-18-937-2021.

Unluata, L.J., Oguz, T., Latif, M.A., Ozsoy, E., 1990. On the physical oceanography of the Turkish Straits. In: Pratt, L.J. (Ed.), The Physical Oceanography of Sea Straits. Kluwer, Dordrecht, pp. 25–60.

Velaoras, V., Krokos, G., Nittis, K., Theocharis, A., 2014. Dense intermediate water outflow from the Cretan Sea: A salinity driven, recurrent phenomenon, connected to thermohaline circulation changes. J. Geophys. Res. Oceans 119, 4797–4820. https://doi.org/10.1002/2014JC009937.

Verri, G., Pinardi, N., Oddo, P., Ciliberti, S.A., Coppini, G., 2018. River runoff influences on the Central Mediterranean overturning circulation. Clim. Dyn. 50, 1675–1703.

Vervatis, V., Skliris, N., Sofianos, S., 2014. Inter-annual/decadal variability of the north Aegean Sea hydrodynamics over 1960–2000. Mediterranean Marine Science 15 (4), 696–705. https://doi.org/10.12681/mms.852.

Wüst, G., 1961. On the vertical circulation of the Mediterranean Sea. J. Geophys. Res. 66, 3261–3271.

Yari, S., Kovačević, V., Cardin, V., Gačić, M., Bryden, H.L., 2012. Direct estimate of water, heat, and salt transport through the Strait of Otranto. J. Geophys. Res. 117, C09009. https://doi.org/10.1029/2012JC007936.

Zervakis V. and D. Georgopoulos, 2002. Hydrology and circulation in the North Aegean (eastern Mediterranean) throughout 1997 and 1998. Hydrology and circulation in the North Aegean (eastern Mediterranean) throughout 1997 and 1998. Mediterranean Marine Science, 3(1), 5-19.

Zodiatis, G., Drakopoulos, P., Brenner, S., Groom, S., 2005. Variability of Cyprus warm core eddy during the CYCLOPS project. Deep-Sea Res. 52, 2897–2910.